Published in final edited form as:
Nat Neurosci. 2020 June 01; 23(6): 730–740. doi:10.1038/s41593-020-0633-7.

Brainstem neurons that command mammalian locomotor asymmetries

Jared M. Cregg[1], **Roberto Leiras**[1], **Alexia Montalant**[1], **Paulina Wanken**[1], **Ian R. Wickersham**[2], **Ole Kiehn**[1,3,*]

[1]Department of Neuroscience, Faculty of Health and Medical Sciences, University of Copenhagen, 2200 Copenhagen, Denmark

[2]The McGovern Institute for Brain Research, Massachusetts Institute of Technology, Cambridge, Massachusetts 02139, USA

[3]Department of Neuroscience, Karolinska Institutet, 17177 Stockholm, Sweden

Abstract

Descending command neurons instruct spinal networks to execute basic locomotor functions, such as which gait and what speed. The command functions for gait and speed are symmetric, implying that a separate unknown system directs asymmetric movements—including the ability to move left or right. Here we report the discovery that *Chx10*-lineage reticulospinal neurons act to control the direction of locomotor movements in mammals. *Chx10* neurons exhibit mainly ipsilateral projection, and their selective unilateral activation causes ipsilateral turning movements in freely moving mice. Unilateral inhibition of *Chx10* neurons causes contralateral turning movements. Paired left/right motor recordings identified distinct mechanisms for directional movements mediated via limb and axial spinal circuits. Finally, we identify sensorimotor brain regions that project onto *Chx10* reticulospinal neurons, and demonstrate that their unilateral activation can impart left/right directional commands. Together these data identify the descending motor system that commands left/right locomotor asymmetries in mammals.

Introduction

Locomotion is a natural behavior universal to the animal kingdom. In vertebrates, coordination of rhythmic locomotor movements occurs largely within circuits of the spinal cord itself[1–4]. For these circuits to function, they need commands from supraspinal effector neurons that control the start and speed of locomotion. The brainstem command neurons which control these parameters have been examined extensively in several vertebrate

*Corresponding author: Ole.Kiehn@sund.ku.dk.

Author contributions

Conceptualization, J.M.C. and O.K.; Methodology, J.M.C., R.L., A.M., and O.K.; Investigation, J.M.C., R.L., A.M., and P.W.; Resources – I.R.W.; Writing – Original Draft, J.M.C. and O.K.; Writing – Review & Editing, J.M.C., R.L., and O.K.; Supervision – O.K.; Funding Acquisition, J.M.C. and O.K.

Competing Interests

The authors declare no competing interests.

Europe PMC Funders Author Manuscripts

species[5–14]. Recently, brainstem neurons that mediate locomotor stop were also identified[7,12,13].

Characteristically, when start command pathways of the midbrain locomotor region are activated unilaterally, they cause bilateral full-bodied locomotion which proceeds in a straight line[7–11,15,16]. This finding underscores symmetry in the command for initiating locomotion and controlling its speed. The anatomical basis for this symmetry has been worked out in some detail. At the level of the midbrain locomotor region, which is comprised of glutamatergic neurons in the cuneiform and pedunculopontine nuclei, neurons exhibit extensive commissural connectivity with neurons of the contralateral side[6,8]. The start command is then relayed bilaterally to reticulospinal neurons[7,8,15], including those of the lateral paragigantocellular nucleus (LPGi), which in turn activate spinal locomotor circuits[7,15,17–20]. Neurons of the LPGi project bilaterally, innervating both sides of the spinal cord, and unilateral optogenetic activation of LPGi glutamatergic neurons initiates symmetric full-bodied locomotion[7].

A considerable gap in our knowledge is the inability to explain how command neurons direct locomotor movements to the left or right side[21]. A system which executes left/right locomotor asymmetries would be required for any goal-directed locomotor movement, as might occur during basic behaviors like foraging, navigation, and/or escape, but also during specialized locomotor tasks[22]. From *in vitro* studies, it is clear that rhythmogenic modules can operate independently within the left or right spinal cord in mammals[23–27]. Nonetheless, differential engagement of left/right rhythmogenic modules cannot be mediated by a symmetric start command. Moreover, unilateral lesion of the corticospinal tract (i.e. unilateral pyramidotomy) does not result in any overt left/right locomotor or postural asymmetries[28,29]. Although unilateral labyrinth ablation or vestibulocochlear nerve (VIII) stimulation can initiate reflexive rotational behavior[30], this self-righting reflex is not considered a voluntary locomotor command.

In the present work, we hypothesized that a turn in mammals could be implemented by a system of nucleus gigantocellularis (Gi) reticulospinal neurons defined by expression of *Chx10* (*Vsx2*)[12]. These *Chx10* Gi neurons are glutamatergic, and their bilateral activation arrests locomotion by suppressing locomotor rhythmogenesis in the spinal cord[12]—however it is unknown whether *Chx10* Gi neurons exhibit symmetric or asymmetric engagement of downstream spinal networks. We found that *Chx10* Gi neurons 1) exhibit dominant unilateral projection to the spinal cord, 2) define the direction of locomotion by effecting changes in ipsilateral limb and axial movements *in vivo*, and 3) can be engaged to impart asymmetric movements via unilateral input from distinct sensorimotor brain regions. *Chx10* Gi neurons exhibit all the features of a *bona fide* system for executing left/right locomotor asymmetries in mammals.

Results

Chx10 Gi neurons form a prominent spinal tract of ipsilaterally projecting axons

For *Chx10* Gi neurons to regulate locomotor movements unilaterally, they should exhibit predominant unilateral projection to the spinal cord. We examined this by labeling *Chx10*-

lineage neurons of the rostral gigantocellularis with an anterograde viral tracer (*Chx10*^{Cre} > AAV-FLEX-tdTomato-2A-synGFP) (Fig. 1a). In adult mice, a unilateral injection labeled *Chx10* Gi neurons mainly on the same side (93.6 ± 3.1%, Fig. 1b-d). *Chx10* neurons projected axons caudally (Extended Data Figs. 1a,b), which then coalesced to form a prominent ipsilateral tract of axons lateral to the inferior olive (Extended Data Fig. 1c). At the level of the pyramidal decussation, this tract of *Chx10* reticulospinal axons turned ventrally to occupy the ipsilateral ventral funiculus within the rostral-most segment of the spinal cord (Extended Data Fig. 1c). TdTomato^{+} axons arborized predominately within the ipsilateral cord (Figs. 1e,f), with some arborizations on the contralateral side.

We quantified the position and density of *Chx10* Gi synGFP^{+} punctae (putative synapses) within the spinal cord. A majority of synGFP^{+} punctae were ipsilateral to the injection site (Figs. 1g,h, Supplementary Table 1). The density of synGFP^{+} punctae was greatest in the ipsilateral intermediate grey (laminae VII, VIII, and X) (Figs. 1g,h), with the exception of Clarke's column (Th1 to L3) (Figs. 1g,h), a medial nucleus which conveys proprioceptive inputs to the cerebellum. Notably, synGFP^{+} punctae were largely absent from dorsal horn laminae I-VI where sensory networks are localized, and from lamina IX where motor neurons reside. These data indicate that *Chx10* reticulospinal neurons likely act on premotor networks[2,12], rather than on motor neurons themselves[12]. We conclude that *Chx10* Gi neurons exhibit mainly ipsilateral projection to the spinal cord, a feature that may allow for differential control of left and right spinal motor networks.

Unilateral excitation of *Chx10* Gi neurons *in vivo* reveals a role in control of asymmetric movements

We next examined the behavioral consequence of unilateral stimulation of *Chx10* Gi neurons in freely moving mice. We expressed excitatory hM3Dq-DREADDs in *Chx10* Gi neurons on one side of the brainstem (Fig. 2a). hM3Dq-DREADDs can be activated with low doses (0.5 mg kg^{-1}) of clozapine-N-oxide (CNO), which causes neuronal depolarization via G_q-mediated signaling[31]. In a cylinder assay, which promotes locomotor turning, we found that CNO administration caused a strong preference in turning toward the side of *Chx10* Gi activation (the ipsilateral side, Fig. 2b). We next examined locomotion in an open field. CNO administration strongly induced ipsilateral turning even during unrestricted, spontaneous locomotion (Fig. 2c, Supplementary Video 1). CNO administration had no behavioral effect in control mice (Extended Data Fig. 2).

Instantaneous analysis of left/right movement preference in the open-field revealed that ipsilateral turning developed over time (Fig. 2d), approaching 100% ipsilateral turning preference by 10 minutes. At early stages following CNO administration (5-15 minutes), these ipsilateral turns were smooth—similar to those observed during spontaneous changes in locomotor direction. There were no clear changes in trunk (axial) posture at early stages following administration of CNO. At late stages (> 20 min), we observed an ipsilateral axial bend which was evident even at rest (Supplementary Video 1). Notably, during both early and late stages following administration of CNO, we only observed changes in locomotor direction when the animal started moving forward, suggesting a specific involvement of the limbs. Analysis of locomotor performance in the open field showed that the average speed

during locomotor bouts decreased following administration of CNO, with no change in the total distance travelled or the number of stops per minute (Extended Data Figs. 3a-d). These data indicate that turns are performed during active locomotion without requiring a locomotor arrest (compare with[12]).

To further investigate the dynamics of this turning behavior, we performed short-lasting photostimulation of *Chx10* Gi neurons after unilateral expression of channelrhodopsin-2 (*Chx10*^{Cre} > AAV-FLEX-ChR2) (Fig. 2e). *Chx10* Gi neurons were stimulated with blue light (473 nm) for 1 s when mice were slowly walking in an open field. Movement trajectories were calculated 1 s before, during, and after stimulation (Fig. 2f). In all cases (42 trials in 7 mice), photostimulation led to an abrupt turn toward the ipsilateral side (Fig. 2f, Supplementary Video 2). This ipsilateral turn was initiated within 150 ms and lasted approximately 1.2 s (Figs. 2g,h), and correlated with a reduction in locomotor speed (Figs. 2h,i). Photostimulation at rest could not evoke a locomotor turn, and instead caused head and trunk bending toward the ipsilateral side (Supplementary Video 2).

These experiments suggest that *Chx10* Gi neurons evoke ipsilateral movements via two distinct mechanisms. Stimulation of *Chx10* Gi neurons at rest evoked ipsilateral head/trunk movements, whereas stimulation during ongoing locomotion caused a reduction in locomotor speed accompanied by movements toward the ipsilateral side. *Chx10* Gi neurons appear to encompass all modes of turning; increasing *Chx10* Gi activity caused changes in trunk posture at rest as well as either gradual and/or sharp changes in locomotor direction.

Unilateral inhibition of *Chx10* Gi neurons *in vivo* causes contralateral movements

We next examined the behavioral consequence of unilateral inactivation of *Chx10* Gi neurons using a Cre-dependent tetanus toxin virus (*Chx10*^{Cre} > AAV-FLEX-TeLC-GFP) (Fig. 3a). In the cylinder assay, we found that FLEX-TeLC (but not FLEX-GFP) injected mice exhibited a strong turning preference toward the contralateral side (Fig. 3b). We performed a time course analysis of turning preference after TeLC injection in the open field. One day before injection of FLEX-TeLC-GFP or FLEX-GFP, mice exhibited no open-field turning preference (Figs. 3c,d, Supplementary Video 3). Mice injected unilaterally with FLEX-TeLC (but not FLEX-GFP) started to exhibit turning contralateral to the injected side as soon as 3 days after injection (Figs. 3c,d). By 9 days, 100% of TeLC mice exhibited contralateral turning (Figs. 3c,d, Supplementary Video 3). Early after TeLC injection, contralateral turns were smooth, and there were no obvious effects on trunk posture at rest (Supplementary Video 3). When the phenotype had fully developed at days 6-9, turns were sharper than in the early stages (Supplementary Video 3). Therefore, similar to unilateral *Chx10* Gi stimulation, inhibition of *Chx10* Gi activity caused both gradual and sharp modes of locomotor turning–but toward the contralateral side. To substantiate these results, we also performed acute inactivation of *Chx10* Gi neurons using inhibitory DREADDS (*Chx10*^{Cre} > FLEX-hM4Di). Similar to chronic inactivation of *Chx10* Gi neurons, acute inactivation promoted contralateral locomotor turning (Fig. 3e-h).

Unilateral inactivation of *Chx10* Gi neurons significantly increased speed and the total distance mice moved during a 30 min probe (Extended Data Figs. 3e-h). There was, however, no change in the number of stops per minute (Extended Data Fig. 3). These data

suggest that *Chx10* Gi neurons act as a unilateral 'brake' on locomotion, and removing this unilateral brake increases locomotor speed and number of turns toward the contralateral side.

Chx10 Gi neurons enable differential control of rhythmic locomotor activity and axial musculature on the left and right sides

We next asked whether ipsilateral projection of *Chx10* Gi neurons can allow for differential control of left and right spinal motor networks using an *in vitro* split-bath preparation (Fig. 4a). Here, locomotor-like hindlimb activity is maintained by adding locomotor promoting drugs (NMDA/5HT) to the lumbar spinal cord while excitatory synaptic activity is blocked in the brainstem (with the broadly acting glutamate receptor blocker, kynurenic acid) (Fig. 4a). Stimulating *Chx10* Gi neurons in this configuration excludes the possibility that locomotor effects are due to axon collaterals acting on local networks in the brainstem[12,32]. In $Chx10^{Cre};R26R^{ChR2}$ preparations, we found that unilateral stimulation of *Chx10* Gi neurons with blue light was unable to evoke a response in lumbar roots. In contrast, during drug-induced locomotor activity, stimulation could decrease the frequency and/or the amplitude of flexor related rhythmic hindlimb locomotor activity on the side ipsilateral to stimulation (ipsi L2, corresponding to reduced swing-phase activity), with little effect on the contralateral side (contra L2) (Fig. 4b-g, $n = 7$, 52 trials). The extensor-related locomotor burst activity on the ipsilateral side (ipsi L5) was prolonged, which corresponds to an increased stance duration (Extended Data Figs. 4a-e, $n = 4$, 33 trials). These observations phenocopy data demonstrating that rhythmicity can be controlled unilaterally in the cord[23,33], and suggest a strong inhibitory effect on rhythm-generating locomotor circuits in the lumbar cord (see also[12]).

The dominant inhibitory effect on hindlimb locomotor rhythmogenesis by *Chx10* Gi stimulation suggests that the descending excitatory signal acts on inhibitory spinal neurons, as previously demonstrated by anterograde tracing[12]. To test this more directly, we blocked inhibitory transmission in the spinal cord using picrotoxin (PTX), a $GABA_A$- and partial glycinergic-receptor blocker. In the presence of PTX (10 μM), the ipsilateral inhibitory effect was blocked ($n = 5$, 69 trials), and sometimes sign-reversed such that stimulation caused L2/L5 excitation (not inhibition, Extended Data Figs. 5a-c). In contrast to the inhibitory effect observed at the lumbar level, unilateral stimulation of *Chx10* Gi neurons caused excitation of thoracic motor neurons that control axial musculature (Extended Data Fig. 5b; $n = 4$, 46 trials), which was PTX-insensitive (Extended Data Fig. 5c). We conclude that *Chx10* Gi neurons can function as a unilateral locomotor effector via unilateral inhibition of locomotor rhythmogenesis. At the thoracic level, however, *Chx10* Gi neurons cause excitation of axial motor neurons.

To investigate this further, we performed *in vivo* experiments with electromyography (EMG) in lightly anesthetized mice. Unilateral *Chx10* Gi stimulation caused a dominant contraction of ipsilateral axial muscles (Figs. 4h-k), including splenius capitis (latency of 14.6 ± 1.0 ms, $n = 5$, ipsilateral head turn) and external abdominal oblique (latency of 23.2 ± 1.7 ms, $n = 3$, ipsilateral trunk bend). In all cases, the dominant movement produced by the stimulus was toward the ipsilateral side; however, in 3 mice there was a negligible EMG response on the contralateral side as well (Figs. 4i,j). Axial muscle activation appeared to be mediated by

Chx10 Gi activation of spinal excitatory neurons (a polysynaptic response) rather than direct monosynaptic activation of motor neurons; axial motor unit recruitment was variable in response to the same stimulus strength and did not follow a high-frequency train with consistent spiking (Fig. 4k). In stark contrast to the excitation of axial muscles, we did not observe any responses from hindlimb flexors or extensors recorded at the same time (Figs. 4h, k). Together the *in vitro* and *in vivo* results indicate a dual effect of ipsilateral *Chx10* Gi activation: ipsilateral excitation of axial muscles (through local excitatory neurons) and ipsilateral inhibition of rhythmic locomotor activity (through local inhibitory neurons).

Limb dynamics during natural and drug-evoked turns

Our data suggests that the mechanism for *Chx10*-evoked locomotor turns reflects distinct changes in limb dynamics: *Chx10*-evoked ipsilateral turns were accompanied by a decrease in locomotor speed (see Figs. 3f,g, Extended Data Fig. 3a), whereas inhibition of *Chx10* Gi neurons caused contralateral turning accompanied by an increase in overall locomotor speed (see Extended Data Fig. 3e).

To investigate these limb dynamics in greater detail, we analyzed how limb coordination relates to locomotor direction in freely moving mice. DeepLabCut was used for markerless extraction of forelimb and hindlimb paw position in an open field (Supplementary Video 4)[34]. We focused on continuous locomotor bouts with a speed >5 cm s^{-1}, which corresponds to walk or trot[35]. For locomotor bouts in wild-type mice, locomotion that proceeded in a straight line exhibited a similar stride length on the left and right sides (Fig. 5a). During spontaneous turns, stride length was reduced on the side of the turn (Fig. 5a). This was true both for the forelimbs and the hindlimbs. We compared spontaneous turns in wild-type mice with those biased to one side via excitation (*Chx10*^{Cre} > hM3Dq-DREADDs after CNO) or inhibition (*Chx10*^{Cre} > FLEX-TeLC) of *Chx10* Gi neurons (Figs. 5b,c). Turns in wild-type mice and those caused by *Chx10*^{Cre} > FLEX-hM3Dq or *Chx10*^{Cre} > FLEX-TeLC shared a defining characteristic, that is, the hindlimbs and the forelimbs on the side of the turn travelled a shorter distance than the leg opposite to the turn (Figs. 5b,c).

We next asked whether differences in stride length between the left and right sides were sufficient to predict locomotor direction (Fig. 5d). For this we examined the relationship between the distance travelled by the right and left limbs and heading direction for all locomotor bouts sampled in wild-type, *Chx10*^{Cre} > FLEX-hM3Dq, and *Chx10*^{Cre} > FLEX-TeLC mice. In wild-type mice, we observed epochs with no difference in left/right stride length, which corresponded to straight walking, as well as epochs with longer left leg steps (turning right) and longer right leg steps (turning left). *Chx10*^{Cre} > FLEX-hM3Dq mice exhibited shorter steps on the side of injection, which caused ipsilateral turns. *Chx10*^{Cre} > FLEX-TeLC mice exhibited longer steps on the side of injection, which caused contralateral turns (Figs. 5e,f, Extended Data Figs. 6a-d). Together these data lead to a model where the difference in stride length on the left and right sides predicts locomotor direction (r^2 = 0.96 for absolute distance, Fig. 5e; r^2 = 0.95 for $\log_2$ ratio, Fig. 5f). These data are compatible with the hypothesis that increased *Chx10* Gi activity reduces the amplitude of locomotor bursts on the ipsilateral side (as observed *in vitro*), leading to shorter steps on the side of the turn.

Chx10 Gi neurons function to control left/right movements during natural exploratory behaviors

To test the necessity/sufficiency of *Chx10* Gi neurons for turns during natural exploratory behaviors, we designed a paradigm where mice explored a novel left- or right-turned maze (Fig. 6a). Mice were placed in the center of this simple spiral-shaped maze, which they explored until they exited the maze or until 10 minutes had elapsed. Unaffected mice rapidly completed both left- and right-turned mazes (Figs. 6a-d). In contrast, unilateral activation of *Chx10* stop neurons with hM3Dq-DREADDs increased exploratory time in a contralateral but not ipsilateral maze (Figs. 6a,b), with several mice failing to complete the contralateral maze altogether (n = 6/8, Fig. 6b). Mirroring this effect, inactivation of *Chx10* stop neurons with TeLC increased exploratory time in an ipsilateral but not contralateral maze (Fig. 6c), with several mice failing to complete the ipsilateral maze (n = 3/8, Fig. 6d). These experiments show that mice do not have an ability to compensate for dysfunction of the *Chx10* turning system, which appears to be required for natural exploratory function.

Neurons of the superior colliculus provide a unilateral input that links *Chx10* Gi neurons to natural left/right movements

These experiments define a final command pathway for executing left/right locomotor asymmetries. The remaining question is whether it is possible to recruit *Chx10* Gi neurons unilaterally during natural behaviors? To address this question, we first performed monosynaptically restricted transsynaptic labeling from *Chx10* Gi neurons to determine their immediate synaptic inputs[36,37]. Cre-dependent rabies helper virus (AAV-FLEX-helper, see methods) was injected in the left Gi of *Chx10*^{Cre} mice, followed by RVΔG-4mCherry(EnvA). Consistent with our results using anterograde tracing (Fig. 1b), monosynaptic retrograde tracing demonstrated that *Chx10* Gi neurons do not exhibit strong connectivity across the midline (Extended Data Figs. 7b,c); *Chx10* Gi neuronal populations are not reciprocally connected. *Chx10* Gi neurons received several long-range inputs that were primarily unilateral from the contralateral superior colliculus (SC), the ipsilateral zona incerta, the ipsilateral mesencephalic reticular formation (mRt) and the contralateral medial cerebellar (the fastigial) nucleus (Fig. 7a and Extended Data Fig. 7, Supplementary Table 2). C*hx10* Gi neurons also exhibited bilateral long-range inputs from the lateral cerebellar (the dentate) nuclei and sensorimotor cortex (Extended Data Fig. 7, Supplementary Table 2). Notably, no transsynaptic labeling was observed from the cuneiform or pedunculopontine nuclei, which comprise the midbrain locomotor region (Supplementary Table 2). These experiments provide anatomical evidence that activity of *Chx10* Gi neurons can be biased via unilateral input from upstream nuclei.

To test this possibility we stimulated the SC-Gi projection. We focused on the SC because of its prominent role in sensorimotor integration[38–40], and for its role in gaze and head orientation within 3D space[41]. Projections from the contralateral SC to Gi have been described[38]. We now show that these SC-Gi projection neurons occupy intermediate layers of the SC, and they synapse specifically with *Chx10* Gi neurons (Fig. 7a,b). We tested the behavioral significance of this SC-Gi projection in four different ways. First, the SC-Gi projection was targeted by retrograde labeling of SC neurons using Gi_{ipsi} > AAV_{retro}-Cre followed by SC_{contra} > FLEX-hM3Dq (Fig. 7c). SC neurons targeted using this approach

had a discrete laminar position which matched the rabies transsynaptic tracing (Figs. 7a,c). In these mice, CNO administration rapidly initiated ipsilateral turning (Fig. 7d). Next, postsynaptic Gi neurons were targeted using SC_{contra} > AAV1-Cre, an anterograde transsynaptic virus[38], followed by Gi_{ipsi} > FLEX-hM3Dq (Fig. 7e). Gi neurons exhibited robust recombination on the ipsilateral side (Fig. 7e). Again, CNO administration rapidly initiated ipsilateral turning (Fig. 7f).

We supplemented these approaches using an intersectional strategy to allow both projection- and target-specific recombination in postsynaptic neurons (Figs. 7g-j). In *Chx10*^{Cre} mice, targeting postsynaptic Gi neurons using SC_{contra} > AAV1-FLEX-FlpO followed by Gi_{ipsi} > dFRT-hM3Dq caused recombination in ipsilateral *Chx10* Gi neurons (Fig. 7g). CNO administration rapidly initiated ipsilateral turning (Fig. 7h). Finally, we showed that SC-Gi projection neurons are glutamatergic. In *Vglut2*^{Cre} (*Slc17a6*) mice[42], glutamatergic SC-Gi projection neurons were targeted using Gi_{ipsi} > AAV_{retro}-FLEX-FlpO followed by SC_{contra} > dFRT-hM3Dq (Fig. 7i). CNO administration rapidly initiated ipsilateral turning (Fig. 7j). These results show that a natural sensorimotor pathway can bias *Chx10* Gi neuronal activity during spontaneous locomotion. Moreover, these experiments unambiguously demonstrate that the SC imparts left/right locomotor directional commands via *Chx10* Gi neurons.

Discussion

The present study uncovers a command system that enables left/right locomotor asymmetries necessary for directional movements. This asymmetric reticulospinal command system functions in parallel with symmetric start and speed control circuits[7–9,11], and may be used symmetrically to arrest ongoing locomotion[12]. Our study, therefore, completes the description of the three main requisite control components for locomotion: start, stop, and direction. Remarkably, when *Chx10* Gi neurons were biased to produce either ipsilateral or contralateral movements, mice could not perform a compensatory turn. This observation suggests that the turning system revealed here is the dominant system used during natural behaviors, and is recruited by brain circuits involved in meditating directional movements.

Mechanism for locomotor turns

In aquatic vertebrates, left/right steering movements are achieved by asymmetric activity of glutamatergic reticulospinal neurons on the left and the right sides. This causes a forceful contraction of axial muscles on the side of the turn[43–46]. In our experiments, we show that asymmetric movements in mice are also caused by an imbalance in descending excitation between the left and right sides, which has a dual effect on spinal circuits: Unilateral *Chx10* Gi neuronal activity 1) causes contraction of the ipsilateral axial muscles and bending of the trunk on the ipsilateral side, and 2) suppresses ipsilateral flexor-related locomotor activity which promotes ipsilateral turning by reducing stride length (force generation) on the ipsilateral side. Thus, excitation in spinal limb locomotor circuits is *reduced* on the side of the turn.

In previous studies we showed that bilateral activation of *Chx10* Gi neurons arrests or reduces limbed locomotor activity via a brake on locomotor rhythmogenesis in the cord[12]. Here we show that unilateral stimulation of *Chx10* Gi neurons reduces the frequency and/or

amplitude of flexor-related hindlimb locomotor activity with a simultaneous prolongation of extensor-related activity. This effect can only be observed during active locomotion, and is suppressed by blocking inhibitory synaptic transmission in the cord. In contrast, unilateral *Chx10* Gi activity leads to activation of axial muscles, observed even at rest, which is insensitive to blockade of inhibitory synaptic transmission in the cord. The mechanisms for these opposing effects, therefore, appears to reflect differential engagement of spinal premotor networks: At the limb level *Chx10* Gi neurons appear to preferentially engage ipsilateral inhibitory networks, whereas at the axial level *Chx10* Gi neurons appear to preferentially engage ipsilateral excitatory networks.

The unilateral *Chx10* Gi gain- and loss-of-function experiments demonstrate that a unilateral brake (activation of *Chx10* Gi neurons) or release of the brake (inactivation of *Chx10* Gi neurons) is essential for mediating a limb-based turn—where speed and stride length are higher on the side opposite to the turn. The reduction in frequency and/or amplitude of flexor-related activity and corresponding prolongation of extensor-related activity observed *in vitro* corresponds well with a unilateral change in step length observed *in vivo*. In many instances, stride length is shortened and locomotor turning is achieved without significant axial bending, which suggests that limb perturbation is a determining factor. Indeed, there is no evidence that axial bending alone is sufficient to initiate a turn as observed in aquatic vertebrates.

We suggest that this turning mechanism for limbed species evolved to account for general features of the limbed body plan. Chiefly, axial muscles generate force perpendicular to the directional axis. In contrast, limbs generate force parallel to the directional axis but at a distance from the midline, creating a moment about the medial axis. Although locomotor direction is ultimately mediated by the limbs and requires locomotion[47], unilateral stimulation of *Chx10* Gi neurons also evoked bending of the head and trunk toward the side of stimulation even at rest. Based on these observations we propose that limbed animals use a two-component system for directing movements to the left or right side. Perhaps not surprisingly, this two-component biological turning system is a design principle adopted for steering four-wheeled vehicles millions of years after it was selected during evolution to control left/right locomotor asymmetries in quadrupeds: turning in quadrupeds and four-wheeled vehicles is enabled by a dedicated steering/differential system for independent control of speed on the left and right sides.

Comparisons with brainstem *Chx10* neurons in aquatic animals

Interestingly, *Chx10* reticulospinal neurons project unilaterally in zebrafish[48], and unilateral ablation of *Chx10* ventral brainstem spinal projection neurons (including nuclei RoV3, MiV1, and MiV2) impairs visually-guided and spontaneous turns[44]. Calcium imaging of these *Chx10* spinal projection neurons revealed that their activity strongly correlated with activity on the side of the turn—that is, on the side of axial muscle contraction. Thus, remarkably, zebrafish and mice both use *Chx10* reticulospinal neurons to transform forward locomotor bouts into movements toward the ipsilateral side. Based on this data, we propose that *Chx10* (Gi) reticulospinal neurons act as a phylogenetically preserved system for imparting directional locomotor commands in all vertebrate species.

Europe PMC Funders Author Manuscripts

Integrated function of *Chx10* Gi neurons

Mammalian *Chx10* Gi neurons were initially associated with locomotor stop, a behavioral response caused by bilateral activation[12]. The data presented here give clear evidence that asymmetric engagement of *Chx10* Gi neurons causes turning. *Chx10* Gi neurons may therefore have a dual function—stop or turn—dependent on their symmetric or asymmetric activation. The basis for differential engagement may rest in task-dependent recruitment from upstream brain areas. Accordingly, our rabies tracing screen demonstrated that certain presynaptic nuclei contribute prominent bilateral or unilateral input. Prominent bilateral inputs from the lateral deep cerebellar nuclei and sensorimotor cortex (among others) provide an anatomical basis for a symmetric stop command. Prominent unilateral input from glutamatergic neurons in the intermediate area of the contralateral superior colliculus, the ipsilateral zona incerta, the ipsilateral mRt, and the contralateral medial deep cerebellar (fastigial) nucleus provide a basis for recruiting an asymmetric turn command. Indeed, we demonstrate that activation of the crossed SC-*Chx10* Gi pathway mediates movements contralateral to the superior colliculus. These experiments clearly demonstrate that *Chx10* Gi neurons can be recruited to generate locomotor asymmetries through the superior colliculus, a hub for sensorimotor integration[38,41].

Interestingly, the superior colliculus, zona incerta, and mRt were recently identified in a brain-wide screen for neurons which control the decision to move left or right[22]. Further, it has been shown that glutamatergic fastigial neurons project to the contralateral Gi[49]. The present brain-wide screen links this excitatory cerebellar output to *Chx10* Gi neurons. Fastigial neurons are downstream of the vestibule-cerebellum, which has been shown to encode turning during locomotion[50]. Glutamatergic inputs from contralateral SC and fastigial neurons to *Chx10* Gi neurons, therefore, contribute information from both sensorimotor and vestibular sources, information which ultimately biases locomotor movements to the ipsilateral side.

Together our findings suggest that *Chx10* Gi neurons act as the final common effector for left/right movements, and might act as a locus for integration of diverse sensorimotor signals which contribute to the decision to move left or right. Understanding the specific contribution of brain areas upstream of *Chx10* Gi neurons—and how they work in concert—is expected to lead to a more thorough understanding of how motor control is organized at the behavioral level.

Online Methods

Mice

All animal experiments and procedures were approved by Dyreforsøgstilsynet in Denmark and the local ethics committee at the University of Copenhagen (Life Sciences Reporting Summary). The $Chx10^{Cre}$ mouse is the same as that used previously[12,51]. The $Vglut2^{Cre}$ mouse is described in[42]. $R26R^{ChR2\text{-}EYFP}$ mice were obtained from Jackson Laboratories (Jackson Stock #012569). For *in vitro* experiments, we used newborn mice from $Chx10^{Cre}$ and $R26R^{ChR2\text{-}EYFP}$ crosses (Life Sciences Reporting Summary). For *in vivo* experiments, we used hemizygous $Chx10^{Cre}$, $Vglut2^{Cre}$, or wild-type mice (C57BL6/J, Jackson Stock

#000664) greater than 8 weeks of age. Experiments were performed with similar numbers of male and female mice.

Stereotaxic Injections

Viral injections in adult mice were performed using a stereotactic injection system (Neurostar, Tübingen, Germany). Mice were anesthetized with 4% isofluorane, and maintained under anesthesia with 2% isofluorane for the duration of the surgery. Anesthetic depth was verified using a toe-pinch test. Virus was mixed with fast green for visualization, and injected using a glass micropipette at a rate of 100 nl min^{-1}. The glass micropipette was held in place for 5 min following injection to prevent backflow.

For unilateral anterograde tracing from Gi to the spinal cord, we injected 250 nl AAV1-phSyn1(S)-FLEX-tdTomato-T2A-SypEGFP-WPRE ($5.56x10^{11}$ ml^{-1}, Viral Vector Core, Salk Institute for Biological Sciences; Addgene #51509)[52] in C*hx10*^{Cre} mice at least 8 weeks of age. Mice were perfused 6 weeks after the injection. All injections in Gi were made at −6.0 mm AP, ± 0.8 mm ML, and −5.5 mm DV relative to bregma.

For experiments using excitatory hM3Dq-DREADDs, C*hx10*^{Cre} mice at least 8 weeks of age were injected in either the left or right Gi with 500 nl of AAV5-hSyn1-DIO-hM3D(Gq)-mCherry-WPRE ($6x10^{12}$ ml^{-1}, Viral Vector Facility, University of Zurich, v89) or 500 nl AAV5-hSyn1-DIO-mCherry control virus ($1.3x10^{13}$ ml^{-1}, Viral Vector Facility, University of Zurich, v116). Experiments were performed 3-6 weeks after injection. *For in vivo* optogenetics experiments, C*hx10*^{Cre} mice were injected with 500 nl of AAVdj-Ef1a-DIO-hChR2(E123T/T159C)-P2A-mCherry-WPRE in the left or right Gi. Optical fibers were implanted 3 weeks later at -6 mm AP, ± 0.5 mm ML, -4.8 mm DV relative to bregma, and photostimulation experiments were performed the next day. For experiments using tetanus toxin virus, we injected either 300 or 500 nl of AAV1-FLEX-TeLC-EGFP to inhibit *Chx10* Gi neurons[12,53], or 500 nl AAV5-FLEX-EGFP as a control. Tetanus toxin behavioral experiments were performed within 9 days of viral injection. For inhibitory DREADDs, *Chx10*^{Cre} mice were injected with 350 nl of AAV5-FLEX-hM4Di-mCherry in the left or right Gi ($7.4x10^{12}$ ml^{-1}, Viral Vector Facility, University of Zurich, v84). Experiments were performed 3-6 weeks after injection.

For rabies transsynaptic labeling, the left Gi was injected with 200 nl of a 1:1 mixture of AAV-syn-FLEX-splitTVA-EGFP-tTA (Addgene #100798) and AAV-TREtight-mTagBFP2-B19G (Addgene #100799)[37]. Seven days later, we injected 500 nl of RVΔG-4mCherry(EnvA) in the same location. Mice were perfused 7 days after the second injection. The synthesis of pAAV-syn-FLEX-splitTVA-EGFP-tTA, pAAV-TREtight-mTagBFP2-B19G, and RVΔG-4mCherry(EnvA) has been described[37,54].

For targeting the SC-Gi projection, injection of AAV-DIO-hM3Dq-mCherry or AAV5-dFRT-hM3Dq-mCherry ($3.5x10^{12}$ ml^{-1}, Viral Vector Facility, University of Zurich, v189-5) was followed 1 week by injection of AAV_{retro}-EGFP-Cre ($1.3x10^{13}$ ml^{-1}, Addgene, 105540-AAVrg), AAV_{retro}-FLEX-EGFP-2A-FlpO ($6.8x10^{12}$ ml^{-1}, Viral Vector Facility, University of Zurich, v171-retro), AAV1-EGFP-Cre ($1x10^{13}$ ml^{-1}, Addgene, 105540-AAV1), or AAV1-FLEX-EGFP-2A-FlpO ($7.3x10^{12}$ ml^{-1}, Viral Vector Facility, University of Zurich, v171-1).

Behavioral experiments were performed 1-2 weeks following second viral injection. For retrograde targeting of SC-Gi projection neurons in wild-type mice, 80 nl of AAV-DIO-hM3Dq-mCherry was injected in the contralateral SC and 150 nl of AAV_{retro}-EGFP-Cre in the ipsilateral Gi. For anterograde targeting of SC-Gi postsynaptic neurons in wild-type mice, 40 nl of AAV1-EGFP-Cre was injected in the contralateral SC and 150 nl of AAV-DIO-hM3Dq-mCherry in the ipsilateral Gi. For retrograde targeting of SC-Gi projection neurons in *Vglut2*^{Cre} mice, 80 nl of AAV-dFRT-hM3Dq-mCherry was injected in the contralateral SC and 150 nl of AAV_{retro}-FLEX-EGFP-2A-FlpO in the ipsilateral Gi. For anterograde targeting of SC-Gi *Chx10* postsynaptic neurons in *Chx10*^{Cre} mice, 80 nl of AAV1-FLEX-EGFP-2A-FlpO was injected in the contralateral SC and 500 nl of AAV-dFRT-hM3Dq-mCherry in the ipsilateral Gi. SC coordinates used for these experiments were based on localization of RVΔG-4mCherry(EnvA) labeled cells[55]: SC: -3.5 mm AP, ± 1.12 mm ML, and −2.15 mm DV relative to bregma.

In Vivo Optogenetics

Optical fibers (200 μm core, NA 0.22, Thorlabs) were implanted 3 weeks after ChR2 viral injection (see information on injection/implantation above). Photostimulation experiments were carried out the day after implantation. Fibers were held in a 1.25 mm ferrule, and coupled to a 473 nm laser (Optoduet, Ikecool Corporation) via a ceramic mating sleeve. Photostimuli were manually triggered via a TTL-pulse given by Ethovision to a Master-8 pulse generator. Laser photostimulation was carried out at 40 Hz (1 s train of 10 ms pulses), where the laser power was adjusted between 5-20 mW to initiate a strong turning response in each animal.

In vivo Electromyography

Chx10^{Cre} mice were injected with 500 nl of AAVdj-Ef1a-DIO-hChR2(E123T/T159C)-P2A-mCherry-WPRE in the left or right Gi and implanted with an optical fibre (200 μm core, 0.22 NA, Thorlabs). Mice were anesthetized intraperitoneally with a cocktail of ketamine (100 mg/kg) and xylazine (10 mg/kg). Body temperature was maintained on a heating pad through the duration of the experiment. Muscles in the neck (splenius capitis), abdomen (abdominal oblique), and hindlimbs (tibialis anterior and soleus) were exposed bilaterally. Two stainless steel wires—teflon-coated except for the tip (Cat. No. 790700, A-M Systems)—were inserted in each muscle for bilateral bipolar electromyographic (EMG) recordings. EMG signals were amplified 5000-10000 times, band-pass filtered from 100 Hz to 1 kHz, sampled at a frequency of 5 kHz (AxoScope, Molecular Devices), and digitally converted (Digidata 1440A, Molecular Devices). Muscle activity was assessed in response to optogenetic stimulation of *Chx10* Gi neurons using a 473 nm laser triggered via a TTL-pulse given by a Master-8 pulse generator. Laser power graded between 5-20 mW, and light stimuli were applied either as a single 20 ms pulse or as a five-pulse train at 50 Hz and 10 ms pulse duration. Data were analysed using Spike2 (Cambridge Electronic Design). When the single pulse stimulation had an effect, 50 Hz stimulation was performed at the same laser power. Multiple recordings were performed in each mouse, and mice were euthanized at the termination of the experiments.

In Vitro Recording and Optogenetics

Locomotor-like activity was recorded from *in vitro* brainstem-spinal cord preparations isolated from P0-4 $Chx10^{Cre};R26R^{ChR2\text{-}EYFP}$ mice. Neonatal mice were anesthetized and decapitated at the level of the midbrain. Mice were then eviscerated, and vertebral bodies were quickly removed ventrally from the level of the rostral pons caudally to the sacral spinal cord under ice-cold oxygenated dissection buffer (95% O_2/5% CO_2, 4 °C) composed of 111 mM NaCl, 3 mM KCl, 26 mM $NaHCO_3$, 1.1 mM KH_2PO_4, 0.25 mM $CaCl_2$, 3.7 mM $MgCl_2$, and 11 mM D-glucose. The ventral roots of were cut at their point of exit from the vertebral canal. The caudal neuroaxis was then isolated from the vertebral canal, and a coronal section was performed at the level of the facial motor nucleus (VII), rostral to the anterior inferior cerebellar artery. The rostral aspect of the preparation was maintained in an upward position to allow access for optical stimulation[12]. Alternatively, the brainstem was split along the midline from the most rostral part to C1. The optical stimulation was then performed unilaterally from the cut surface.

A two-compartment system was used for pharmacological separation of the brainstem and lumbar spinal cord. The preparation was pinned to a Sylgard stage, and Vaseline was applied to the upper thoracic spinal cord at ~Th1. A peristaltic pump was used to separately perfuse the rostral (brainstem) and caudal (lumbar spinal cord) compartments with oxygenated recording buffer (95% O_2/5% CO_2, 22-24 °C), composed of 111 mM NaCl, 3 mM KCl, 26 mM $NaHCO_3$, 1.1 mM KH_2PO_4, 2.5 mM $CaCl_2$, 1.25 mM $MgCl_2$, and 11 mM D-glucose. Kynurenic acid (KA, 4 mM; Sigma) was applied to the brainstem compartment to block all glutamatergic transmission in the brainstem, thereby isolating the contribution of *Chx10* reticulospinal neurons to spinal circuits[12]. A cocktail of *N*-methyl-D-aspartic acid (NMDA, 6-8 μM; Sigma) and serotonin (5HT, 6-15 μM; Sigma), and sometimes with dopamine (DA, 50-100 μM; Sigma) was applied to the lumbar spinal cord compartment to initiate locomotor-like activity. Fast green dye was maintained within the rostral compartment to verify an intact diffusion barrier, that is, drugs from the rostral compartment did not mix with the caudal compartment and *vice versa*.

Bipolar suction electrodes were attached to the left and right L2 and L5 ventral roots, and/or to the left and right thoracic ventral roots. The signals were amplified 5000-10000 times, band-pass filtered from 100 Hz to 1 kHz and sampled at a frequency of 1 kHz with AxoScope (Molecular Devices). Optogenetic stimulation of ChR2-expressing neurons was performed using a 473 nm laser system (UGA-40; Rapp Optoelectronic), which delivered blue light at an intensity of 30 mW mm^{-2} [56]. Blue light was directed at the preparation using an optical fiber (200 μm core, 0.22 NA, Thorlabs). Photo illumination was carried out continuously for 2-5 s. Frequency of locomotor like activity and burst amplitude (Figs. 4f,g) were analyzed from rectified, integrated (bin = 0.25 s) traces (using Spike2; Cambridge Electronic Design), where we quantified those bursts occurring 10 s before, 5 s during, and 10 s after light stimulation. 5-11 trials were quantified for each animal. To generate intensity plots for individual trials, rectified and integrated traces were exported, and then normalized in amplitude from 0 (representing the minimum time-series value in a trial) to 1 (maximum value).

To block inhibition in the spinal cord, picrotoxin (5-10 μM; Sigma) was added to the caudal pool in the presence locomotor-inducing drugs.

Limb Dynamics

DeepLabCut[34,57] was used for markerless extraction of paw position in an openfield. DeepLabCut 2.0 was installed on a PC equipped with a GEforce RTX 2080 Ti graphics card. We captured videos of mice moving from below (50 f.p.s.). Body center position was tracked using Ethovision XT, and video segments were extracted for locomotor bouts directed through the center of the arena that were >5 cm s^{-1} and >15 cm long. The four paws, the tip of the nose, and the base of the tail were tracked using DeepLabCut 2.0. 700 frames were selected for labeling from videos representing different behavioral sessions. The network was trained for 600,000 iterations until the loss reached a plateau. Segments of recording with likelihood <0.9 for any marker were excluded.

Subsequent analyses of limb kinematics were made using custom scripts in Python 3.7. The body angle was defined as tail base-nose angle relative to the x axis. The velocity of each paw was used to define steps. Steps were first detected as consecutive points where paw velocity passed above/below 25 cm s^{-1}. The detection was further refined by defining the beginning of the swing phase as the point where paw velocity passed above 9 cm s^{-1}, and the end of the swing phase (i.e., the beginning of the stance phase) as the point where paw velocity passed back below 9 cm s^{-1}. During alternating gaits including fast walk and trot, mice move forward through the environment using diagonals—i.e. one forelimb and the contralateral hindlimb. Diagonal steps were defined as those occurring the closest in time for diagonal limbs. For each step, stride length was calculated as the length of the segment between the beginning and the end of the swing phase. We compared differences in stride length between the left and right sides with body angle at the beginning and end of a diagonal step. Pearson's correlation coefficient was used to estimate how stride length correlated with body angle.

Tissue Immunochemistry & Imaging

Mice were euthanized by anesthetic overdose with pentobarbital (250 mg/kg), and perfused transcardially with 4°C saline followed by 4% paraformaldehyde. Brain and spinal cord tissue was dissected free, and then post-fixed in 4% paraformaldehyde for 3 h at 4 °C. Tissue was cryoprotected by incubation in 30% sucrose in phosphate buffered saline (PBS) overnight. Tissue was then embedded in Neg-50 medium (ThermoFisher Scientific) for cryostat sectioning. Coronal or sagittal sections were obtained on a Leica cryostat and mounted on Superfrost Plus slides (ThermoFisher Scientific). Brainstem coronal sections were cut at 30 μm thickness, whereas spinal cord coronal sections were cut at 20 μm. Sagittal sections were cut at 30 μm.

Sections were rehydrated for 5 minutes in PBS + 0.5% Triton-X100 (PBS-T; Sigma-Aldrich), and then blocked for 2 h in 10% normal donkey serum in PBS-T (Jackson ImmunoResearch). Sections were incubated overnight with primary antibodies diluted in blocking solution. We used the following primary antibodies: chicken anti-GFP (1:1000, Abcam, ab13970) and rabbit anti-DsRed/tdTomato/mCherry (1:1000, Clontech, 632496)

Europe PMC Funders Author Manuscripts

The specificity of primary antibodies was validated in previous publications as indicated in the Antibody Registry (Life Sciences Reporting Summary). Slides were washed 4 times in PBS-T, and then incubated with appropriate donkey secondary antibodies diluted in blocking solution (1:500, ThermoFisher Scientific). Slides were washed 4 times in PBS-T, counterstained with Hoechst 33342 (1:2000) or NeuroTrace 435 (1:400, ThermoFisher Scientific), and were mounted with coverslips using mowiol 4-88 medium. Sections were imaged using either a Zeiss widefield epifluorescence microscope or a Zeiss LSM 780 confocal microscope.

Drugs

Clozapine-N-oxide (CNO, Tocris, 4936) was dissolved in saline immediately prior to behavioral experiments. CNO was administered intraperitoneally at a dose of 0.5 mg kg^{-1} (*Chx10*^{Cre} > FLEX-hM3Dq; Fig. 2, Extended Data Figs. 2, 3, and 6) or 1 mg kg^{-1} (*Chx10*^{Cre} > FLEX-hM4Di, Fig. 3; SC or Gi > FLEX-hM3Dq or dFRT-hM3Dq, Fig. 7).

Cylinder Test

Mice were placed in a 15 cm diameter cylinder for 10 minutes. Ethovision XT (Noldus) software was used to capture video (15 f.p.s.) and carry out tracking of head, center point, and tail. 360° clockwise and counterclockwise revolutions were quantified (tail point to center point, 50° threshold).

Open Field

Mice were acclimated to the behavioral suite prior to testing in an open field arena. Open field analysis was carried out in a 50 x 50 cm square arena illuminated with an infrared lamp. Ethovision XT (Noldus) software was used to capture video (15-25 f.p.s.) and carry out tracking analysis. Mice were tracked using head, center, and tail points, enabling quantification of rotations as a function of time. Movement parameters taken in the open field included 360° revolutions (tail point to center point, 50° threshold), velocity of locomotor bouts (bouts of locomotion were defined as periods during which the animal moved at a velocity greater than 2 cm s^{-1}), total movement (m), ambulation (time moving at a velocity greater than 2 cm s^{-1}), and stops per minute (instances where velocity fell below 2 cm s^{-1}). Tracking was carried out for 60 minutes. Mice were allowed to acclimate to the arena for 30 min, followed by a 30 min probe. Movement parameters are reported for minutes 30-60.

Ipsilateral/Contralateral Spiral Maze

Spiral-shaped mazes were used to test clockwise/counterclockwise movement preference. For this purpose, mazes were fabricated which could be explored from the center-point to the periphery only by moving in a clockwise or counterclockwise direction (see Figs. 6a,c for illustration). These mazes exhibit an increasing radius as mice move from the center-point to the periphery. For each mouse, a 10 minute trial was conducted in either the left- or right-turned maze. One affected mouse exhibited a turning radius that was smaller than the center of the maze (see Figs. 6a,c). This affected mouse was excluded from analysis because

Europe PMC Funders Author Manuscripts

it could not complete either the ipsilateral or contralateral maze. Body tracking was carried out with Ethovision XT using center-point detection.

Analysis

For quantification of viral transduction in Gi, the number of neurons ipsilateral and contralateral to the injection site was counted in every 10th section. These counts were used to estimate the percentage of viral transduction contained to the ipsilateral side (Fig. 1). Similar analysis was performed to estimate the percentage of labeled neurons in the ipsilateral versus contralateral superior colliculus (Fig. 7).

For analysis of synGFP^{+} punctae in tdTom-2A-synGFP traced projections, high resolution images of GFP-stained coronal spinal cord sections were obtained with a confocal microscope. Three images from each spinal level (i.e. cervical, thoracic, lumbar) were quantified from three mice. Analysis of synGFP punctae was restricted to the grey matter, with the assumption that synGFP punctae in white matter reflected transport of synGFP protein rather than *bona fide* synapses. SynGFP punctae were isolated from the images using thresholding, and the position of each punctum was extracted using the particle analysis feature in ImageJ (https://imagej.nih.gov/ij/). The position of the central canal was defined using the Nissl counterstain, and synGFP punctae position was normalized between sections and mice using this point as a reference. From this data set, the percentage of synapses ipsilateral and contralateral to the injection site was estimated (Fig. 1). Synaptic density plots were constructed in R, where gradation represents the range from zero to maximum density at each spinal level (Fig. 1g). Synaptic density plots represent the average of 6 mice. Coordinates and abbreviations are based on Paxinos and Franklin's reference atlas[55], and corresponding plates are from the Allen Mouse Brain Atlas[58].

Statistics

No statistical methods were used to pre-determine sample sizes; our sample sizes are similar to those reported in previous publications(Life Sciences Reporting Summary)[8,59,60]. Mice were randomly allocated to different groups for the *in vivo* experiments using a block design. Data collection and analysis were not performed blind to the conditions of the experiments - but the analysis was automated so that the experimenter had no influence on the outcome. Mice that did not react to experimental perturbations (CNO or light) were excluded from analysis only if it was confirmed that the viral infection was not present or off target. This exclusion was done post-experimentally since it required analysis of tissue from the animal. A paired two-tailed t-test was performed for pairwise comparisons. For multiple comparisons, a one-, two-, or three-way ANOVA (with repeated measures where appropriate) was performed to determine whether significant differences existed between conditions, followed by multiple comparisons testing using Tukey-Kramer HSD. Data distribution was assumed to be normal but this was not formally tested. An *F*-test was used to determine significance in regression analyses. Data are plotted with box-and-whisker plots which give the median, 25th and 75th percentiles, and the range. Time-series data tracking movement preference in the open field and individual *n* in linear regression are given as mean ± standard error mean. Individual data points are plotted for each comparison, and information on statistical analyses, *P* value statistics, and *n* values are listed in the figure

legend, as well as in Supplementary Table 1. *n* values represent distinct biological replicates (mice), except for regression analyses in Extended Data Fig. 6 where *n* represents individual steps or locomotor bouts. The number of trials varied between mice. $P < 0.05$ was considered statistically significant, where $*P < 0.05$, $**P < 0.01$, and $***P < 0.001$. Statistical analyses were carried out in Graphpad Prism 8.3 or SAS JMP Pro 15.

Extended Data

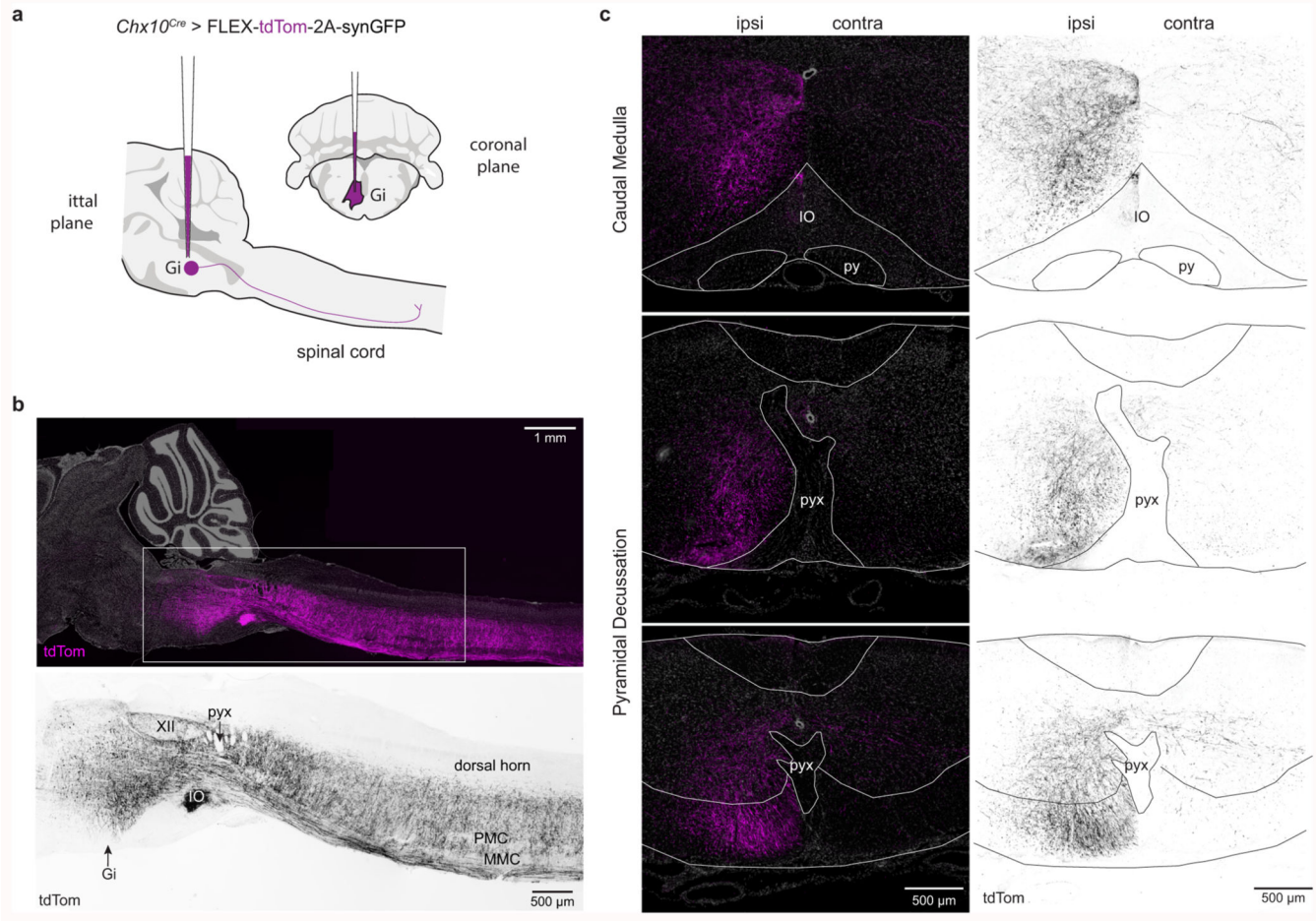

Extended Data Fig. 1. *Chx10* Gi neurons form a prominent tract of ipsilaterally projecting axons. **a**, Unilateral labeling of *Chx10* neurons of the rostral gigantocellularis (Gi) using the Cre-dependent anterograde tracer AAV-FLEX-tdTom-2A-synGFP. **b**, *Top*, Sagittal section of $tdTom^+$ projections ipsilateral to the injection site. $tdTom^+$ axons formed a prominent tract that projected caudally to the spinal cord. *Bottom*, inset from *Top*. XII, hypoglossal motor nucleus; pyx, pyramidal decussation; IO, inferior olive; PMC, phrenic motor column; MMC, medial motor column. Images in (**b**) are representative of tracing experiments from $n = 3$ mice. **c**, Coalescence of *Chx10* reticulospinal axons dorsal to the inferior olive (*top*), and subsequent positioning in the ventrolateral funiculus at the level of the pyramidal decussation (*bottom*). Images in (**c**) are representative of tracing experiments from $n = 6$ mice.

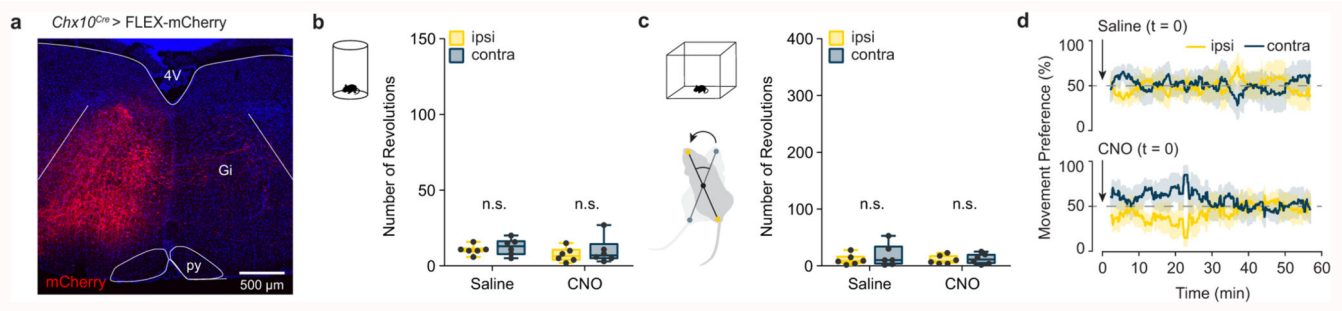

Extended Data Fig. 2. CNO administration does not affect turning preference in control AAV-mCherry injected mice.

a, Example of mCherry expression 3 weeks after a 500 nl unilateral injection of AAV-FLEX-mCherry in a *Chx10*^{Cre} mouse (representative image from $n = 6$ mice). mCherry expression is confined to the side ipsilateral to injection. **b**, Turning preference in a 10 minute cylinder assay is unaffected by administration of CNO. $P > 0.24$ (see Supplementary Table 1), two-way ANOVA with Tukey's multiple comparisons test, $n = 6$ mice from one experiment. **c**, Turning preference in an open field arena is unaffected by administration of CNO. $P > 0.42$, two-way ANOVA with Tukey's multiple comparisons test, $n = 6$ mice from one experiment. Box-and-whisker plots in (**c**,**d**) give the median, 25th and 75th percentiles, and range. **d**, Instantaneous quantification of ipsilateral and contralateral revolutions for mice in (**c**) after injection of either saline or CNO in AAV-FLEX-mCherry injected mice. Time-series data are plotted as mean ± standard error mean.

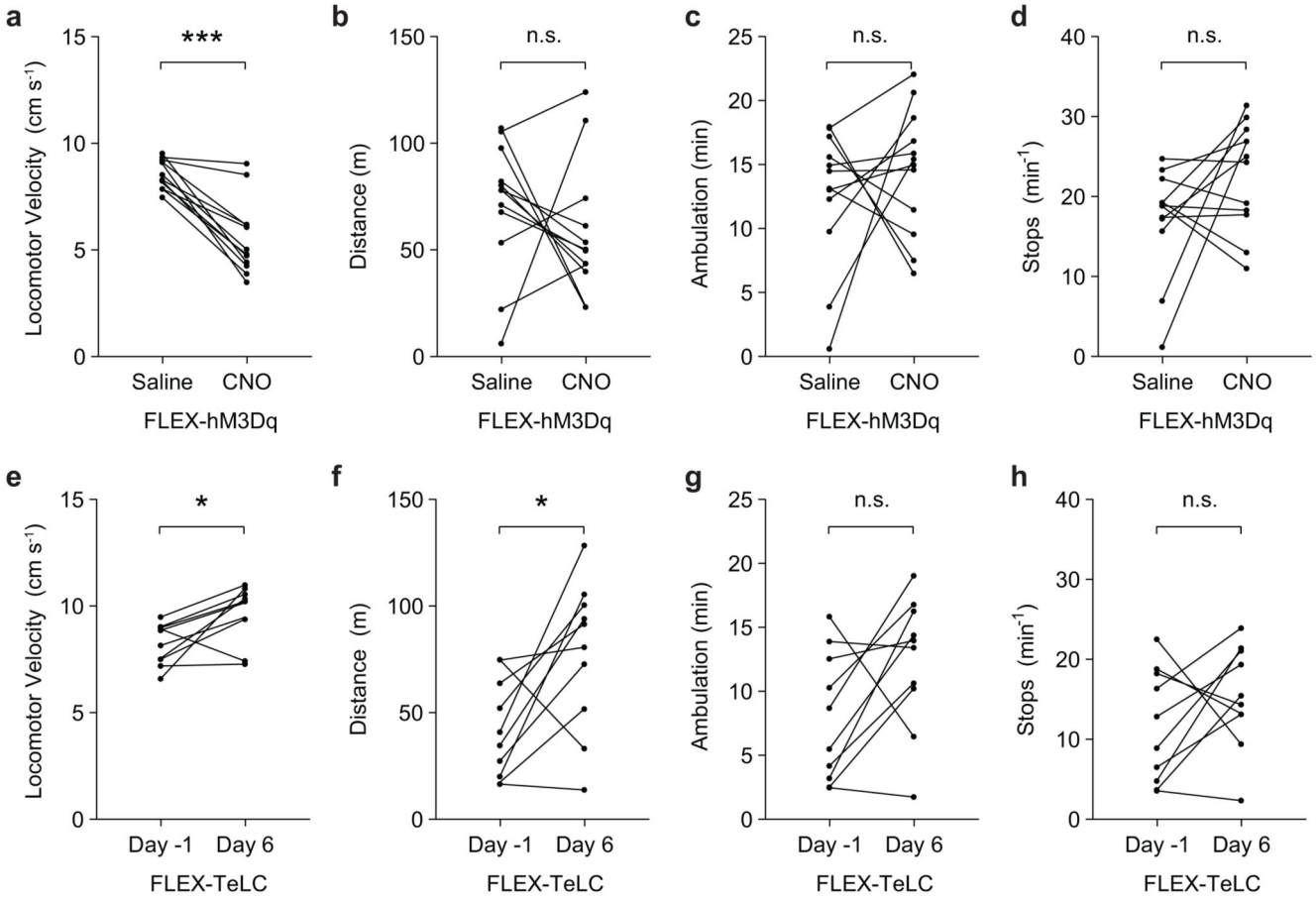

Extended Data Fig. 3. Analysis of open field locomotor performance in *Chx10*^{Cre} > FLEX-hM3Dq and *Chx10*^{Cre} > FLEX-TeLC mice.

a-d, Open field locomotor performance in *Chx10*^{Cre} > FLEX-hM3Dq mice after administration of saline or CNO. CNO administration significantly decreased the velocity of locomotor bouts (**a**, ***$P < 0.001$, paired two-tailed t-test, $n = 12$ mice from three independent experiments), with no effect on the distance traveled (**b**, $P = 0.40$, paired two-tailed t-test, $n = 12$ mice), ambulation (**c**, $P = 0.46$, paired two-tailed t-test, $n = 12$ mice), or number of stops per minute (**d**, $P = 0.11$, paired two-tailed t-test, $n = 12$ mice). **e-h**, Open field locomotor performance in *Chx10*^{Cre} > FLEX-TeLC mice 1 day before injection versus 6 days after injection. TeLC expression significantly increased the velocity of locomotor bouts (**e**, *$P = 0.015$, paired two-tailed t-test, $n = 10$ mice from two independent experiments) and the distance traveled (**f**, *$P = 0.022$, paired two-tailed t-test, $n = 10$ mice from two independent experiments), with no effect on ambulation (**g**, $P = 0.07$, paired two-tailed t-test, $n = 10$ mice) or the number of stops per minute (**h**, $P = 0.24$, paired two-tailed t-test, $n = 10$ mice).

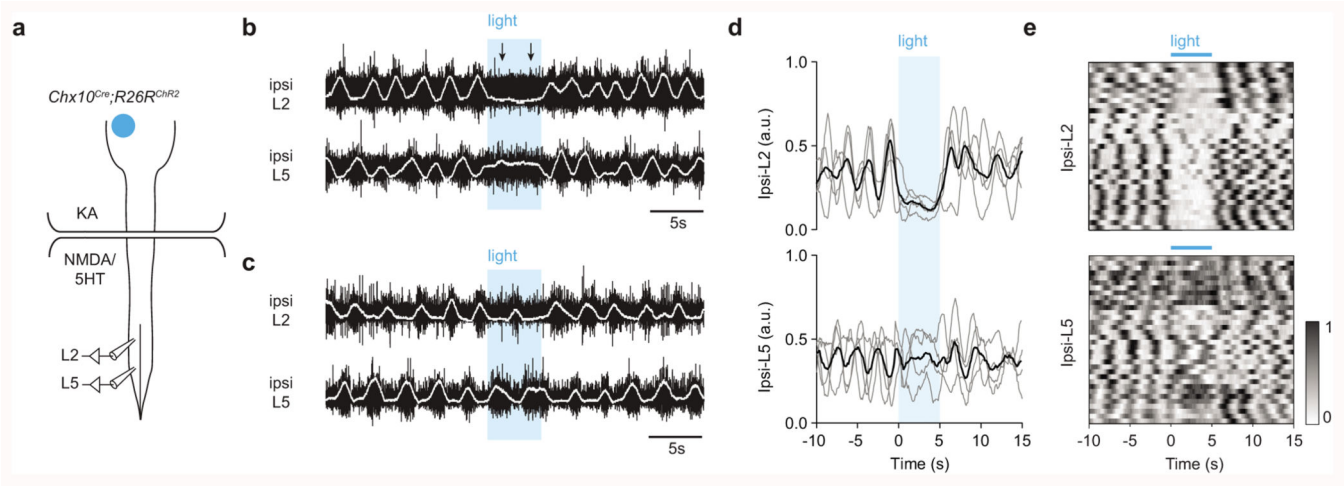

Extended Data Fig. 4. Unilateral activation of *Chx10* Gi neurons causes inhibition of ipsilateral rhythmic flexor locomotor activity and prolongation of ipsilateral extensor locomotor activity.

a, Schematic of split-bath brainstem-spinal cord preparation from P0-4 *Chx10*^{Cre};*R26R*^{ChR2} mice, as in Fig. 4. Recordings are taken from the ipsilateral L2 (flexor-related) and L5 (extensor-related) ventral roots. **b-c**, Unilateral photostimulation of *Chx10* Gi neurons reduces the frequency (**b**) and/or the amplitude (**c**) of locomotor-like flexor activity ipsilateral (ipsi L2) to the stimulation (compare with Fig. 4), with a simultaneous prolongation of extensor-related burst duration (ipsi L5). Traces in (**b**,**c**) are derived from two different mice and are representative of $n = 4$ independent preparations. **d**, Integrated traces normalized in amplitude from 0-1 and averaged across trials for each mouse ($n = 4$ mice, grey), with the grand average across mice represented in black. **e**, 33 trials from 4 mice represented as intensity plots from 0-1, which are integrated traces normalized from 0-1. 3 of the mice represented for ipsi-L2 are also represented in Fig. 4.

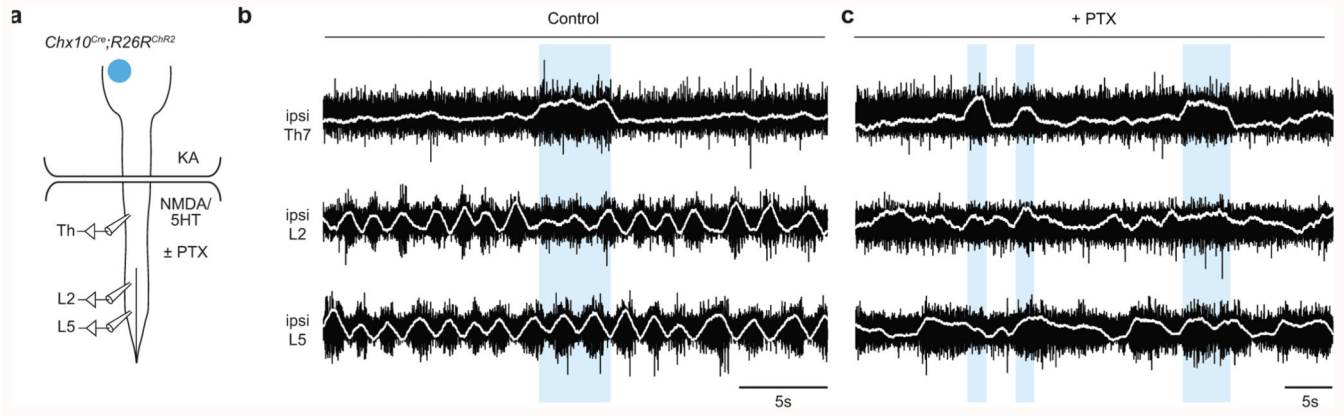

Extended Data Fig. 5. Blocking inhibition in the spinal cord reveals an opposite effect of *Chx10* Gi stimulation on axial and locomotor networks.

a, Schematic of split-bath brainstem-spinal cord preparation from P0-P4 *Chx10*^{Cre};*R26R*^{ChR2} mice, as in Fig. 4. Recordings are taken from the ipsilateral thoracic (Th, axial), L2 (flexor-related), and L5 (extensor-related) ventral roots. Picrotoxin (PTX, 10 μM) was added to the caudal pool to block inhibition in the spinal cord. **b**, Recordings from

Europe PMC Funders Author Manuscripts

Europe PMC Funders Author Manuscripts

ipsilateral Th7, L2, and L5 ventral roots in presence of NMDA/5HT demonstrating that unilateral photostimulation of *Chx10* Gi neurons reduces the locomotor-like flexor activity ipsilateral (ipsi L2) to the stimulation, with a simultaneous prolongation of extensor-related burst durations (ipsi L5), and a tonic increase of thoracic activity lasting for the stimulus duration. (*n* = 4 independent preparations, 46 trials). **c**, In the presence of PTX, photostimulation of *Chx10* Gi neurons no longer affected rhythmic lumbar locomotor-like activity (*n* = 5 independent preparations, 69 trials), whereas activation of thoracic (axial) motor activity is still present.

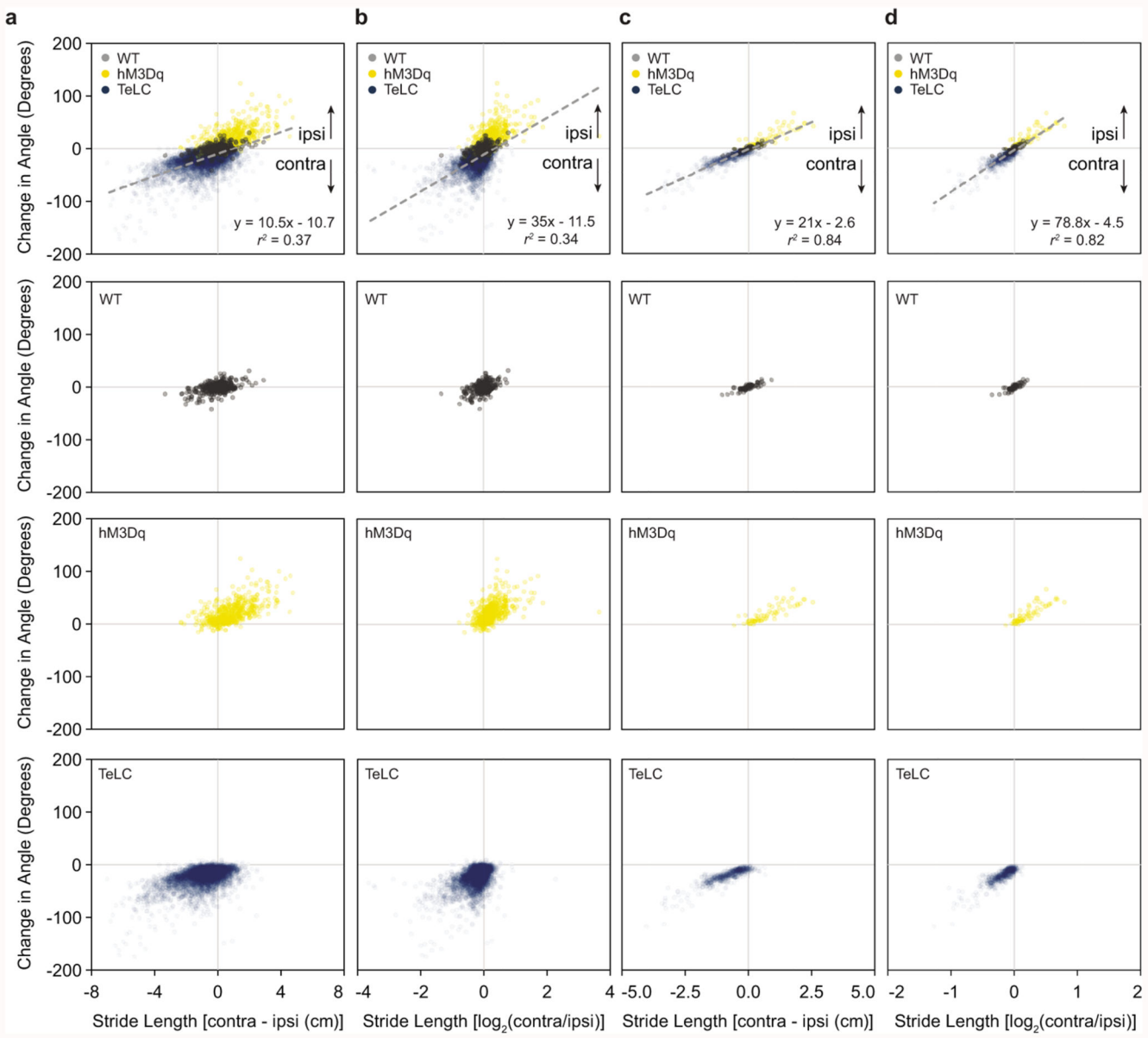

Extended Data Fig. 6. Stride length asymmetries versus heading position in wild-type, *Chx10*^{Cre} > FLEX-hM3Dq, and *Chx10*^{Cre} > FLEX-TeLC mice.

Europe PMC Funders Author Manuscripts

a-b, Analysis of individual steps relative to direction of movement in wild-type (WT), *Chx10*^{Cre} > FLEX-hM3Dq (hM3Dq), and *Chx10*^{Cre} > FLEX-TeLC (TeLC) mice. Stride length (cm) was measured on the ipsilateral and contralateral side together with the direction of movement. Stride length values are positive when the stride length is longer on the contralateral side. Positive changes in angle reflect an ipsilateral turn whereas negative values are contralateral. 6016 individual steps were analyzed from 6 wildtype (WT) (352 strides), 6 hM3Dq (477 strides), and 6 TeLC (5187 strides) mice. ***$P < 0.001$ for regression in (**a**) and (**b**), F-test, $n = 6016$ strides. **c-d**, Data for individual locomotor bouts (representing the average of all steps in a locomotor bout) from WT, hM3Dq, and TeLC mice. 708 locomotor bouts were analyzed from 6 WT (63 bouts), 6 hM3Dq (61 bouts), and 6 TeLC (584 bouts) mice. ***$P < 0.001$ for regression in (**c**) and (**d**), F-test, $n = 708$ locomotor bouts. Full information on regression analyses for WT, hM3Dq, TeLC, and pooled data can be found in Supplementary Table 1. Goodness of fit is given as the coefficient of determination (r^2; the square of Pearson's r).

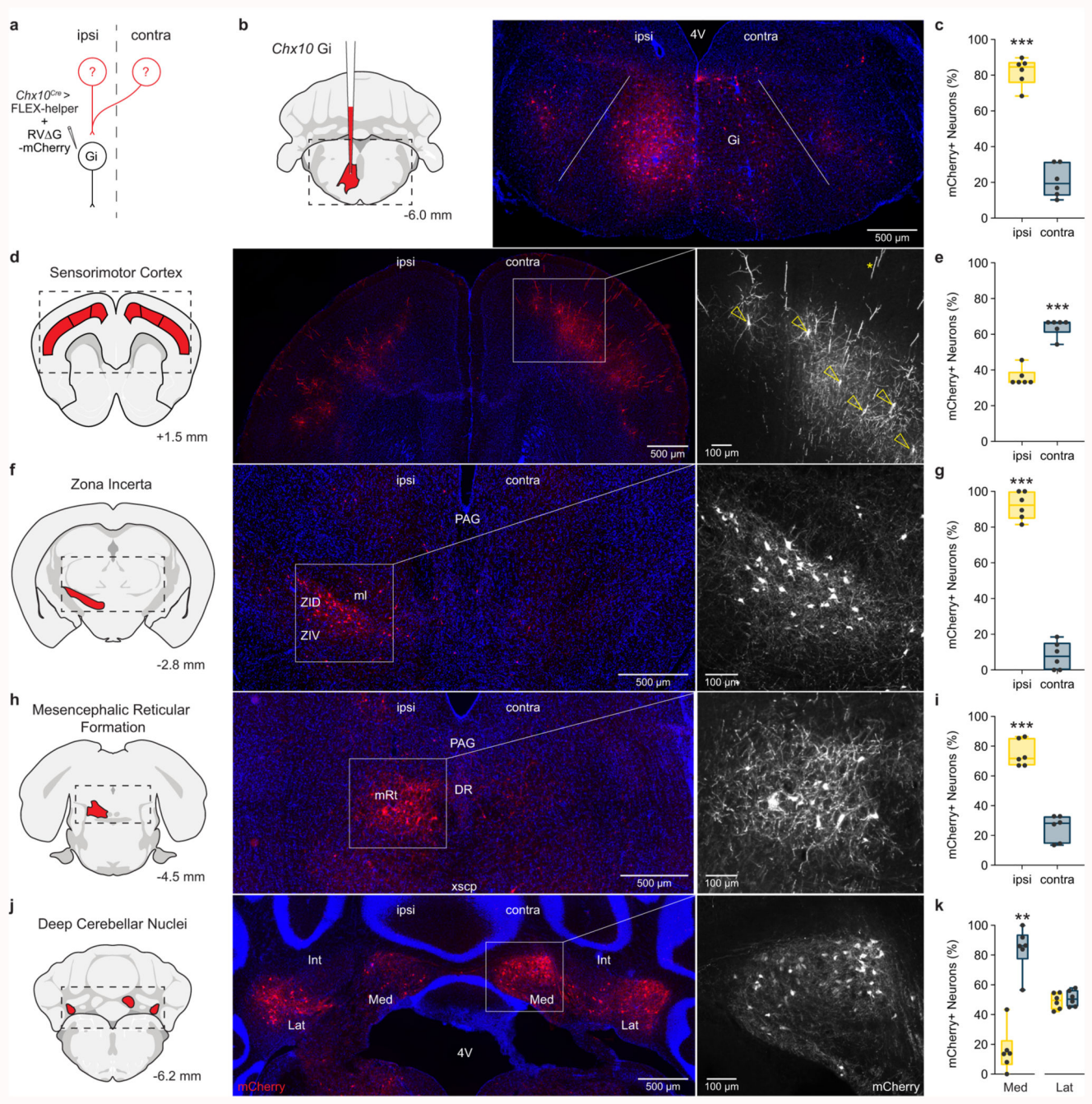

Extended Data Fig. 7. Monosynaptic rabies tracing identifies *Chx10* Gi presynaptic inputs.

a, A rabies transsynaptic tracing approach was used to identify presynaptic inputs to *Chx10* Gi neurons (see also, Fig. 7 and Supplementary Table 2). **b**, Injection site in rostral Gi. Initial site of infection is visualized as a large population of mCherry^{+} neurons, accompanied by dense mCherry^{+} processes. Starter neurons of the ipsilateral Gi do not exhibit a strong input from neurons of the contralateral Gi. **c**, Quantification of mCherry-labeled neurons in the ipsilateral and contralateral Gi. ***$P = 0.0002$, paired two-tailed t-test, $n = 6$ mice from one experiment. **d**, Bilateral input to *Chx10* Gi neurons from neurons

Europe PMC Funders Author Manuscripts

of primary motor and somatosensory cortex. Open yellow triangles point to soma from pyramidal neurons. Yellow asterisk indicates an apical dendrite. **e**, Quantification of mCherry-labeled neurons in the ipsilateral and contralateral cortex. ***$P = 0.001$, paired two-tailed t-test, $n = 6$ mice from one experiment. **f**, Input to *Chx10* Gi neurons from neurons of the ipsilateral zona incerta. Presynaptic neurons were observed primarily in the dorsal (ZID) and caudal aspects of the zona incerta. **g**, Quantification of mCherry-labeled neurons in the ipsilateral and contralateral zona incerta. ***$P < 0.001$, paired two-tailed t-test, $n = 6$ mice from one experiment. **h**, Unilateral input to Chx10 Gi neurons from the ipsilateral mesencephalic reticular formation. **i**, Quantification of mCherry-labeled neurons in the ipsilateral and contralateral mesencephalic reticular formation. ***$P = 0.001$, paired two-tailed t-test, $n = 6$ mice from one experiment. **j**, Medial (Med) and lateral (Lat) deep cerebellar nuclei exhibited unilateral or bilateral, respectively, input to *Chx10* Gi neurons. **k**, Quantification of mCherry-labeled neurons in the deep cerebellar nuclei. Med, **$P = 0.0024$, paired two-tailed t-test, $n = 6$ mice from one experiment; Lat, $P = 0.69$, paired two-tailed t-test, $n = 6$ mice from one experiment. Box-and-whisker plots in (**c**,**e**,**g**,**i**,**k**) give the median, 25th and 75th percentiles, and range.

Supplementary Material

Refer to Web version on PubMed Central for supplementary material.

Acknowledgements

We thank K. Sharma, L. Zagoraiou, S. Crone, and T.M. Jessell for the *Chx10*^{Cre} mouse. We acknowledge the Core Facility for Integrated Microscopy, Faculty of Health and Medical Sciences, University of Copenhagen. We thank Iryna Vesth-Hansen and Dorthe Meinertz for technical assistance, and members of Ole Kiehn's lab for discussion and comments on previous versions of this manuscript. This work was supported by an EMBO Long-Term Fellowship (J.M.C., ALTF 421-2018), the European Research Council (ERC) under the European Union's Horizon 2020 research and innovation program (OK, grant agreement No REP-SCI-693038), the Novo Nordisk Laureate Program (O.K., NNF15OC0014186), and The Faculty of Health and Medical Sciences (O.K.).

Data Availability

The data that support the findings of this study are available from the corresponding author upon reasonable request.

Code Availability

The code used to analyze data and produce figure content is available from the corresponding author upon request.

References

1. Grillner S. The motor infrastructure: from ion channels to neuronal networks. Nat Rev Neurosci. 2003; 4:573–586. [PubMed: 12838332]
2. Kiehn O. Decoding the organization of spinal circuits that control locomotion. Nat Rev Neurosci. 2016; 17:224–238. [PubMed: 26935168]
3. Goulding M. Circuits controlling vertebrate locomotion: moving in a new direction. Nat Rev Neurosci. 2009; 10:507–518. [PubMed: 19543221]

4. Brownstone RM, Wilson JM. Strategies for delineating spinal locomotor rhythm-generating networks and the possible role of Hb9 interneurones in rhythmogenesis. Brain Res Rev. 2008; 57:64–76. [PubMed: 17905441]
5. Jordan LM, Liu J, Hedlund PB, Akay T, Pearson KG. Descending command systems for the initiation of locomotion in mammals. Brain Res Rev. 2008; 57:183–191. [PubMed: 17928060]
6. Ryczko D, Dubuc R. The multifunctional mesencephalic locomotor region. Curr Pharm Des. 2013; 19:4448–70. [PubMed: 23360276]
7. Capelli P, Pivetta C, Soledad Esposito M, Arber S. Locomotor speed control circuits in the caudal brainstem. Nature. 2017; 551:373–377. [PubMed: 29059682]
8. Caggiano V, et al. Midbrain circuits that set locomotor speed and gait selection. Nature. 2018; 553:455–460. [PubMed: 29342142]
9. Josset N, et al. Distinct Contributions of Mesencephalic Locomotor Region Nuclei to Locomotor Control in the Freely Behaving Mouse. Curr Biol. 2018; 28:884–901.e3. [PubMed: 29526593]
10. Musienko PE, et al. Spinal and Supraspinal Control of the Direction of Stepping during Locomotion. J Neurosci. 2012; 32:17442–17453. [PubMed: 23197735]
11. Roseberry TK, et al. Cell-Type-Specific Control of Brainstem Locomotor Circuits by Basal Ganglia. Cell. 2016; 164:526–537. [PubMed: 26824660]
12. Bouvier J, et al. Descending Command Neurons in the Brainstem that Halt Locomotion. Cell. 2015; 163:1191–1203. [PubMed: 26590422]
13. Juvin L, et al. A Specific Population of Reticulospinal Neurons Controls the Termination of Locomotion. Cell Rep. 2016; 15:2377–2386. [PubMed: 27264174]
14. Grillner S, et al. Intrinsic function of a neuronal network - a vertebrate central pattern generator. Brain Res Brain Res Rev. 1998; 26:184–97. [PubMed: 9651523]
15. Brocard F, et al. The transformation of a unilateral locomotor command into a symmetrical bilateral activation in the brainstem. J Neurosci. 2010; 30:523–33. [PubMed: 20071515]
16. Shik ML, Severin FV, Orlovskii GN. Control of walking and running by means of electric stimulation of the midbrain. Biofizika. 1966; 11:659–66. [PubMed: 6000625]
17. Shefchyk SJ, Jell RM, Jordan LM. Reversible cooling of the brainstem reveals areas required for mesencephalic locomotor region evoked treadmill locomotion. Exp brain Res. 1984; 56:257–62. [PubMed: 6479262]
18. Garcia-Rill E, Skinner RD. The mesencephalic locomotor region. I. Activation of a medullary projection site. Brain Res. 1987; 411:1–12. [PubMed: 2440511]
19. Garcia-Rill E, Skinner RD. The mesencephalic locomotor region. II. Projections to reticulospinal neurons. Brain Res. 1987; 411:13–20. [PubMed: 3607422]
20. Bachmann LC, et al. Deep brain stimulation of the midbrain locomotor region improves paretic hindlimb function after spinal cord injury in rats. Sci Transl Med. 2013; 5
21. Ferreira-Pinto MJ, Ruder L, Capelli P, Arber S. Connecting Circuits for Supraspinal Control of Locomotion. Neuron. 2018; 100:361–374. [PubMed: 30359602]
22. Steinmetz NA, Zatka-Haas P, Carandini M, Harris KD. Distributed coding of choice, action and engagement across the mouse brain. Nature. 2019; doi: 10.1038/s41586-019-1787-x
23. Hagglund M, et al. Optogenetic dissection reveals multiple rhythmogenic modules underlying locomotion. Proc Natl Acad Sci. 2013; 110:11589–11594. [PubMed: 23798384]
24. Kjaerulff O, Kiehn O. Distribution of networks generating and coordinating locomotor activity in the neonatal rat spinal cord in vitro: a lesion study. J Neurosci. 1996; 16:5777–5794. [PubMed: 8795632]
25. Bracci E, Ballerini L, Nistri A. Localization of rhythmogenic networks responsible for spontaneous bursts induced by strychnine and bicuculline in the rat isolated spinal cord. J Neurosci. 1996; 16:7063–7076. [PubMed: 8824342]
26. Bonnot A, Whelan PJ, Mentis GZ, O'Donovan MJ. Locomotor-like activity generated by the neonatal mouse spinal cord. Brain Res Brain Res Rev. 2002; 40:141–51. [PubMed: 12589913]
27. Kremer E, Lev-Tov A. Localization of the Spinal Network Associated With Generation of Hindlimb Locomotion in the Neonatal Rat and Organization of Its Transverse Coupling System. J Neurophysiol. 1997; 77:1155–1170. [PubMed: 9084588]

28. Muir GD, Whishaw IQ. Complete locomotor recovery following corticospinal tract lesions: measurement of ground reaction forces during overground locomotion in rats. Behav Brain Res. 1999; 103:45–53. [PubMed: 10475163]
29. Jin D, et al. Restoration of skilled locomotion by sprouting corticospinal axons induced by co-deletion of PTEN and SOCS3. Nat Commun. 2015; 6
30. Deliagina TG, Popova LB, Grant G. The role of tonic vestibular input for postural control in rats. Arch Ital Biol. 1997; 135:239–61. [PubMed: 9177127]
31. Armbruster BN, Li X, Pausch MH, Herlitze S, Roth BL. Evolving the lock to fit the key to create a family of G protein-coupled receptors potently activated by an inert ligand. Proc Natl Acad Sci. 2007; 104:5163–5168. [PubMed: 17360345]
32. Hägglund M, Borgius L, Dougherty KJ, Kiehn O. Activation of groups of excitatory neurons in the mammalian spinal cord or hindbrain evokes locomotion. Nat Neurosci. 2010; 13:246–252. [PubMed: 20081850]
33. Kjaerulff O, Kiehn O. Crossed rhythmic synaptic input to motoneurons during selective activation of the contralateral spinal locomotor network. J Neurosci. 1997; 17:9433–47. [PubMed: 9390999]
34. Mathis A, et al. DeepLabCut: markerless pose estimation of user-defined body parts with deep learning. Nat Neurosci. 2018; 21:1281–1289. [PubMed: 30127430]
35. Bellardita C, Kiehn O. Phenotypic Characterization of Speed-Associated Gait Changes in Mice Reveals Modular Organization of Locomotor Networks. Curr Biol. 2015; 25:1426–1436. [PubMed: 25959968]
36. Wall NR, Wickersham IR, Cetin A, De La Parra M, Callaway EM. Monosynaptic circuit tracing in vivo through Cre-dependent targeting and complementation of modified rabies virus. Proc Natl Acad Sci. 2010; 107:21848–21853. [PubMed: 21115815]
37. Liu K, et al. Lhx6-positive GABA-releasing neurons of the zona incerta promote sleep. Nature. 2017; 548:582–587. [PubMed: 28847002]
38. Zingg B, et al. AAV-Mediated Anterograde Transsynaptic Tagging: Mapping Corticocollicular Input-Defined Neural Pathways for Defense Behaviors. Neuron. 2017; 93:33–47. [PubMed: 27989459]
39. Shang C, et al. A parvalbumin-positive excitatory visual pathway to trigger fear responses in mice. Science. 2015; 348:1472–1477. [PubMed: 26113723]
40. Felsen G, Mainen ZF. Neural Substrates of Sensory-Guided Locomotor Decisions in the Rat Superior Colliculus. Neuron. 2008; 60:137–148. [PubMed: 18940594]
41. Oliveira AF, Yonehara K. The Mouse Superior Colliculus as a Model System for Investigating Cell Type-Based Mechanisms of Visual Motor Transformation. Front Neural Circuits. 2018; 12:59. [PubMed: 30140205]
42. Borgius L, Restrepo CE, Leao RN, Saleh N, Kiehn O. A transgenic mouse line for molecular genetic analysis of excitatory glutamatergic neurons. Mol Cell Neurosci. 2010; 45:245–257. [PubMed: 20600924]
43. Fagerstedt P, Orlovsky GN, Deliagina TG, Grillner S, Ullén F. Lateral Turns in the Lamprey. II. Activity of Reticulospinal Neurons During the Generation of Fictive Turns. J Neurophysiol. 2001; 86:2257–2265. [PubMed: 11698516]
44. Huang KH, Ahrens MB, Dunn TW, Engert F. Spinal projection neurons control turning behaviors in zebrafish. Curr Biol. 2013; 23:1566–73. [PubMed: 23910662]
45. Kozlov AK, Kardamakis AA, Hellgren Kotaleski J, Grillner S. Gating of steering signals through phasic modulation of reticulospinal neurons during locomotion. Proc Natl Acad Sci U S A. 2014; 111:3591–6. [PubMed: 24550483]
46. Thiele TR, Donovan JC, Baier H. Descending control of swim posture by a midbrain nucleus in zebrafish. Neuron. 2014; 83:679–91. [PubMed: 25066082]
47. Gruntman E, Benjamini Y, Golani I. Coordination of steering in a free-trotting quadruped. J Comp Physiol A Neuroethol Sens Neural Behav Physiol. 2007; 193:331–45. [PubMed: 17146663]
48. Kimura Y. alx, a Zebrafish Homolog of Chx10, Marks Ipsilateral Descending Excitatory Interneurons That Participate in the Regulation of Spinal Locomotor Circuits. J Neurosci. 2006; 26:5684–5697. [PubMed: 16723525]

49. Bagnall MW, et al. Glycinergic Projection Neurons of the Cerebellum. J Neurosci. 2009; 29:10104–10110. [PubMed: 19675244]
50. Muzzu T, Mitolo S, Gava GP, Schultz SR. Encoding of locomotion kinematics in the mouse cerebellum. PLoS One. 2018; 13
51. Azim E, Jiang J, Alstermark B, Jessell TM. Skilled reaching relies on a V2a propriospinal internal copy circuit. Nature. 2014; 508:357–363. [PubMed: 24487617]
52. Oh SW, et al. A mesoscale connectome of the mouse brain. Nature. 2014; 508:207–214. [PubMed: 24695228]
53. Murray AJ, et al. Parvalbumin-positive CA1 interneurons are required for spatial working but not for reference memory. Nat Neurosci. 2011; 14:297–299. [PubMed: 21278730]
54. Wickersham IR, Sullivan HA. Rabies viral vectors for monosynaptic tracing and targeted transgene expression in neurons. Cold Spring Harb Protoc. 2015; doi: 10.1101/pdb.prot072389
55. Franklin KBJ, Paxinos G. Paxinos and Franklin's The mouse brain in stereotaxic coordinates.
56. Bellardita C, et al. Spatiotemporal correlation of spinal network dynamics underlying spasms in chronic spinalized mice. Elife. 2017; 6
57. Nath T, et al. Using DeepLabCut for 3D markerless pose estimation across species and behaviors. Nat Protoc. 2019; 14:2152–2176. [PubMed: 31227823]
58. Lein ES, et al. Genome-wide atlas of gene expression in the adult mouse brain. Nature. 2007; 445:168–176. [PubMed: 17151600]
59. Jennings JH, et al. Interacting neural ensembles in orbitofrontal cortex for social and feeding behaviour. Nature. 2019; 565:645–649. [PubMed: 30651638]
60. Evans DA, et al. A synaptic threshold mechanism for computing escape decisions. Nature. 2018; 558:590–594. [PubMed: 29925954]

Europe PMC Funders Author Manuscripts

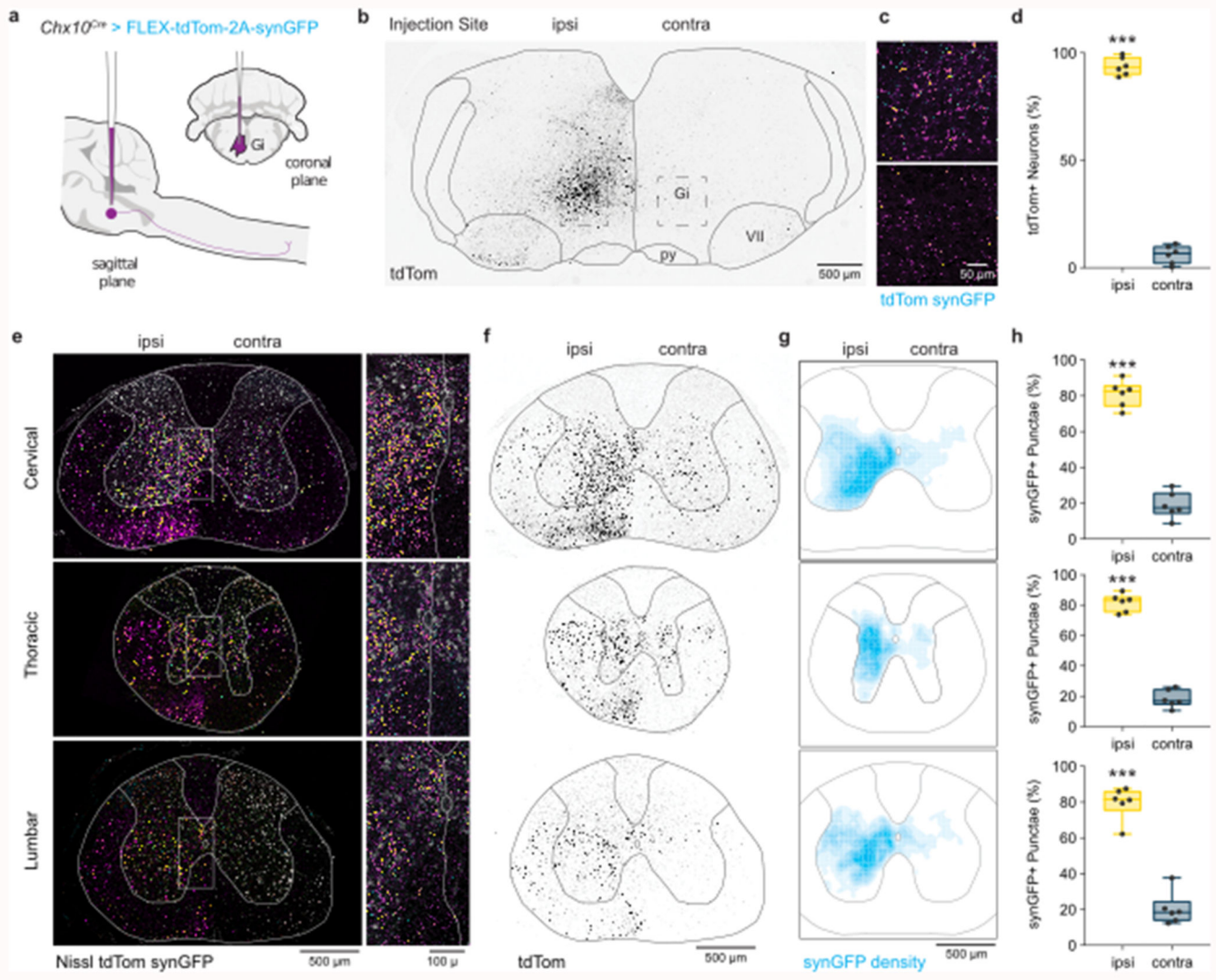

Fig. 1. *Chx10* Gi neurons form a prominent tract of descending axons that project ipsilaterally.

a, Unilateral labeling of *Chx10* neurons of the rostral gigantocellularis (Gi) using the Cre-dependent anterograde tracer AAV-FLEX-tdTom-2A-synGFP. **b**, Inverted fluorescent image of tdTomato$^+$ neurons at the injection site within Gi. **c**, *Top*, tdTom$^+$/synGFP$^+$ neurons at injection site. *Bottom*, sparse tdTom$^+$ axonal labeling and synGFP$^+$ punctae contralateral to the injection site. **d**, Quantification of tdTom$^+$ neurons labeled ipsilateral (ipsi) and contralateral (contra) to the injection site. ***$P < 0.001$, paired two-tailed t-test, $n = 6$ mice from two independent experiments. **e**, *Left*, A prominent tract of tdTom$^+$ axons is observed within the ventrolateral funiculus of the cervical (top), thoracic (middle), and lumbar (bottom) spinal cord. Axons project almost exclusively on the ipsilateral side. SynGFP$^+$ punctae (overlap of cyan with magenta yields yellow) exhibit a high density on the ipsilateral side. *Right*, Insets from images on left demonstrate a sharp division in the density of axon profiles and synGFP$^+$ punctae between the ipsilateral and contralateral sides. **f,** Inverted fluorescent images of tdTom$^+$ axonal projections in the cervical (top), thoracic (middle), and lumbar (bottom) spinal cord. Axons descend in the ventrolateral funiculus

within a well-defined “wedge”. **g**, Density plots for synGFP$^+$ punctae within the grey matter of the cervical (top), thoracic (middle), and lumbar (bottom) spinal cord (average from 6 mice). The density of putative synapses is greatest in the intermediate grey matter—laminae VII, VIII, and X. SynGFP$^+$ punctae were found predominantly on the ipsilateral side, and excluded from laminae I-VI of the dorsal horn, lamina IX (motor neurons), and at the thoracic level, Clarke’s column. Scale bar = 500 μm. **h**, Quantification of synGFP$^+$ punctae within the ipsilateral and contralateral spinal cord grey matter. Cervical, ***$P = 0.001$; Thoracic, ***$P < 0.001$; Lumbar, ***$P < 0.001$. Paired two-tailed t-test, $n = 6$ mice from two independent experiments. Data are plotted with box-and-whisker plots which give the median, 25th and 75th percentiles, and range.

Europe PMC Funders Author Manuscripts

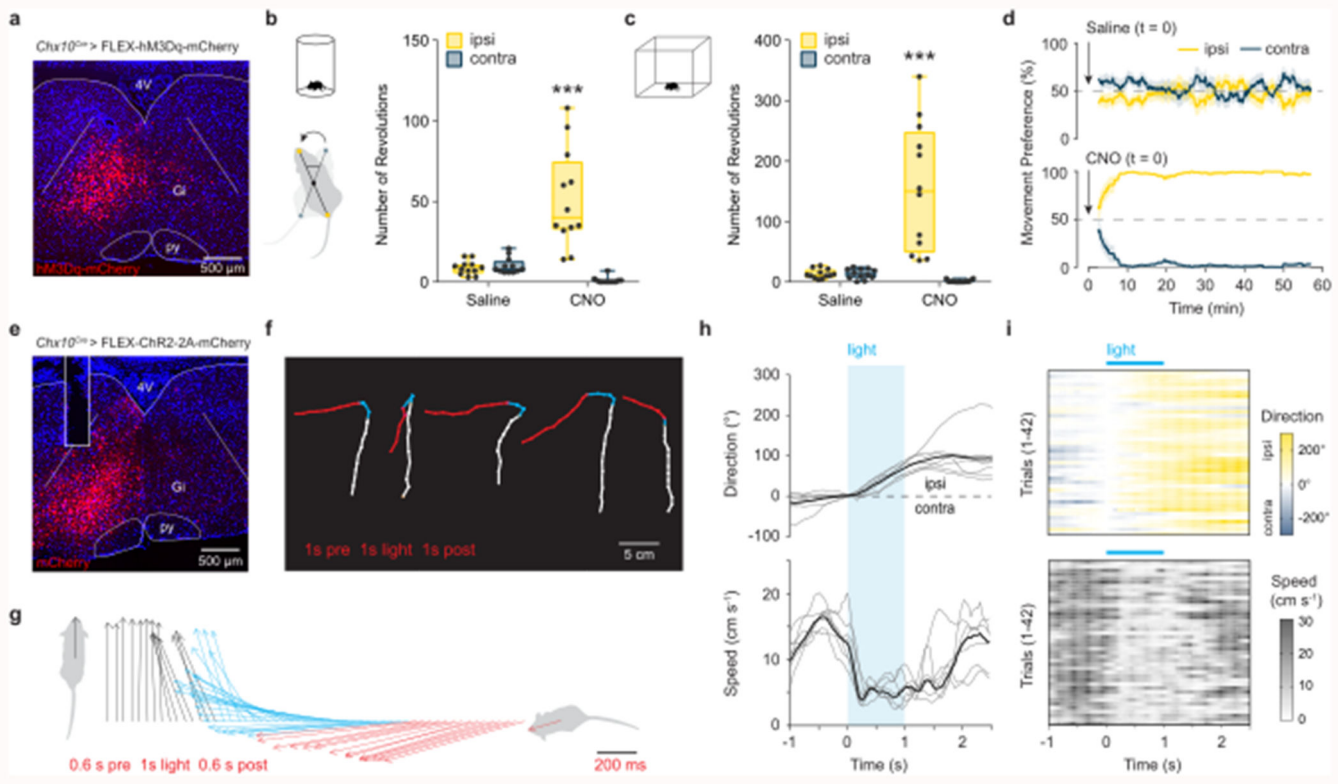

Fig. 2. Excitation of *Chx10* Gi neurons causes ipsilateral movements.

a, Unilateral infection of *Chx10* Gi neurons with AAV-FLEX-hM3Dq-mCherry. **b**, Turning preference in a cylinder assay 1 h after injection of saline or CNO, quantified as the total number of revolutions over a 10 min trial. ***$P < 0.001$, two-way ANOVA with Tukey's multiple comparisons test, $n = 12$ mice from three independent experiments. **c**, Movement preference in an open field assay, quantified between 30-60 min post-injection of saline or CNO. ***$P < 0.001$, two-way ANOVA with Tukey's multiple comparisons test, $n = 12$ mice from three independent experiments. Box-and-whisker plots in (**b**,**c**) give the median, 25th and 75th percentiles, and range. **d**, Instantaneous analysis of movement preference for mice in (**c**), quantified as the percentage of ipsilateral versus contralateral revolutions (bin = 5 min), following injection of saline (*top*) or CNO (*bottom*) at t = 0. Data are plotted as mean ± standard error mean. **e**, Unilateral injection of AAV-FLEX-ChR2-2A-mCherry in *Chx10*^{Cre} mice. Example of mCherry expression and optical fiber placement in Gi. **f**, Body tracking 1 s before (white), 1 s during (blue), and 1 s following (red) light stimulation. Representative examples are plotted from 5 different mice ($n = 7$ mice total from two independent experiments). The distance travelled during stimulation is reduced compared to before and after stimulation. **g**, Body center-to-head vectors were plotted as a function of time 0.6 s before (black), 1 s during (blue), and 0.6 s following (red) light stimulation for 1 representative mouse ($n = 7$ mice total). **h**, Quantification of movement direction and speed relative to light onset. Photostimulation caused an abrupt shift in movement direction toward the ipsilateral side, accompanied by a reduction in locomotor speed. Grey traces represent the mean for each mouse, whereas the black trace represents the mean calculated across all

mice, $n = 7$. **i**, 42 individual trials plotted from $n = 7$ mice in two independent experiments, 3-9 trials per mouse.

Europe PMC Funders Author Manuscripts

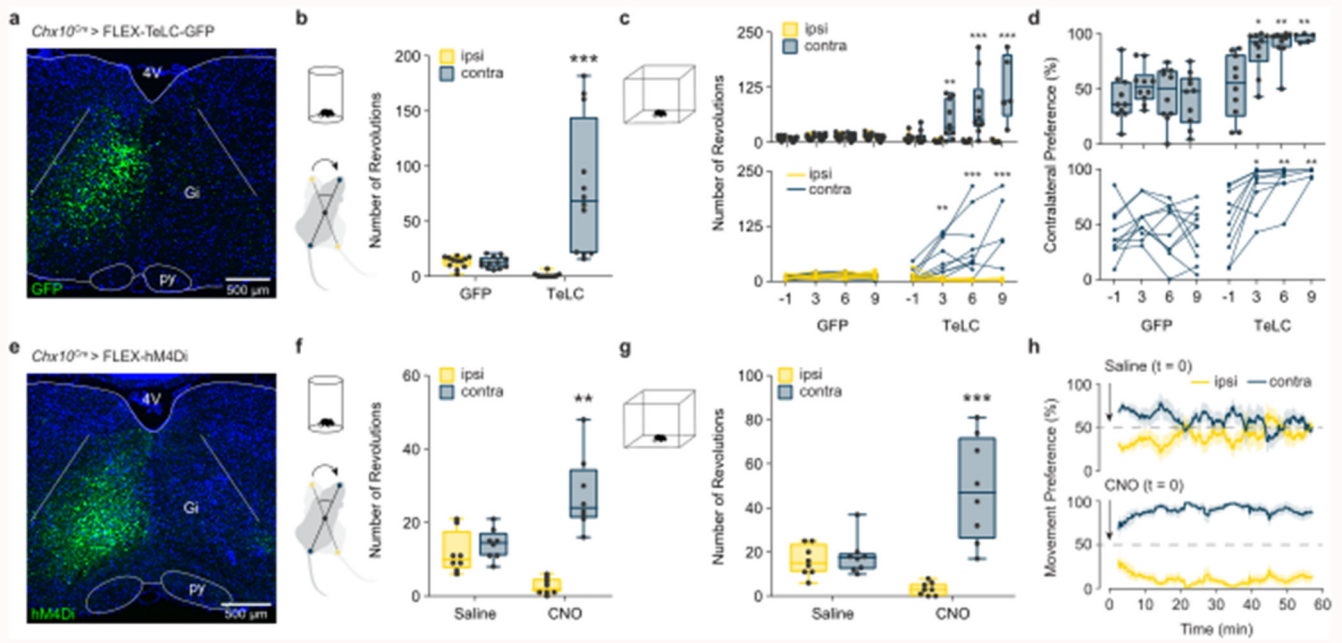

Fig. 3. Inhibition of *Chx10* Gi neurons causes contralateral movements.

a, Unilateral injection of AAV-FLEX-TeLC-GFP or AAV-FLEX-GFP in *Chx10*^{Cre} mice. Example of GFP expression in Gi two weeks post-injection. **b**, Turning preference in a cylinder assay 7 d after viral injection, quantified as the total number of revolutions over a 10 min trial. ***$P < 0.001$, two-way ANOVA with Tukey's multiple comparisons test, $n =$ 12 mice from three independent experiments. **c**, Turning preference in an open field assay, quantified as the total number of revolutions during a 30 min trial. **$P = 0.0046$, day 3 TeLC ipsi vs. contra; ***$P < 0.001$, day 6 TeLC ipsi vs. contra; ***$P < 0.001$, day 9 TeLC ipsi vs. contra (see Supplementary Table 1). Three-way ANOVA with Tukey's multiple comparisons test. $n = 10$ mice from two independent experiments for GFP days -1, 3, 6, and 9. $n = 10$ mice from two independent experiments for TeLC days -1, 3, and 6. $n = 5$ mice for TeLC day 9. The top panel gives the box-and-whisker distribution for each group, whereas the bottom panels gives the phenotypic progression in each animal. **d**, Turning preference in an open field assay, quantified as the percentage of total revolutions during a 30 min trial. *$P = 0.0211$, day 3 vs. day -1 TeLC; **$P = 0.003$, day 6 vs. day -1 TeLC; **$P = 0.0067$, day 9 vs. day -1 TeLC. Two-way ANOVA with Tukey's multiple comparisons test. $n = 10$ mice for GFP days -1, 3, 6, and 9. $n = 10$ mice for TeLC days -1, 3, and 6. $n = 5$ mice for TeLC day 9 (see Supplementary Table 1). Box-and-whisker plots in (**b**-**d**) give the median, 25th and 75th percentiles, and range. **e**, Example of hM4Di expression after unilateral injection of AAV-FLEX-hM4Di in *Chx10*^{Cre} mice. **f**, Turning preference in a cylinder assay 20 min after injection of saline or CNO, quantified as the total number of revolutions over a 10 min trial. **$P = 0.0011$, two-way ANOVA with Tukey's multiple comparisons test, $n = 8$ mice from two independent experiments. **g**, Turning preference in an open field assay, quantified between 30-60 min post-injection of saline or CNO. ***$P < 0.001$, two-way ANOVA with Tukey's multiple comparisons test, $n = 8$ mice from two independent experiments. Box-and-whisker plots in (**f**,**g**) give the median, 25th and 75th percentiles, and range. **h**, Instantaneous analysis of movement preference for mice in (**g**), quantified as the percentage of ipsilateral

versus contralateral revolutions (bin = 5 min), following injection of saline (*top*) or CNO (*bottom*) at t = 0. Data are plotted as mean ± standard error mean.

Europe PMC Funders Author Manuscripts

Europe PMC Funders Author Manuscripts

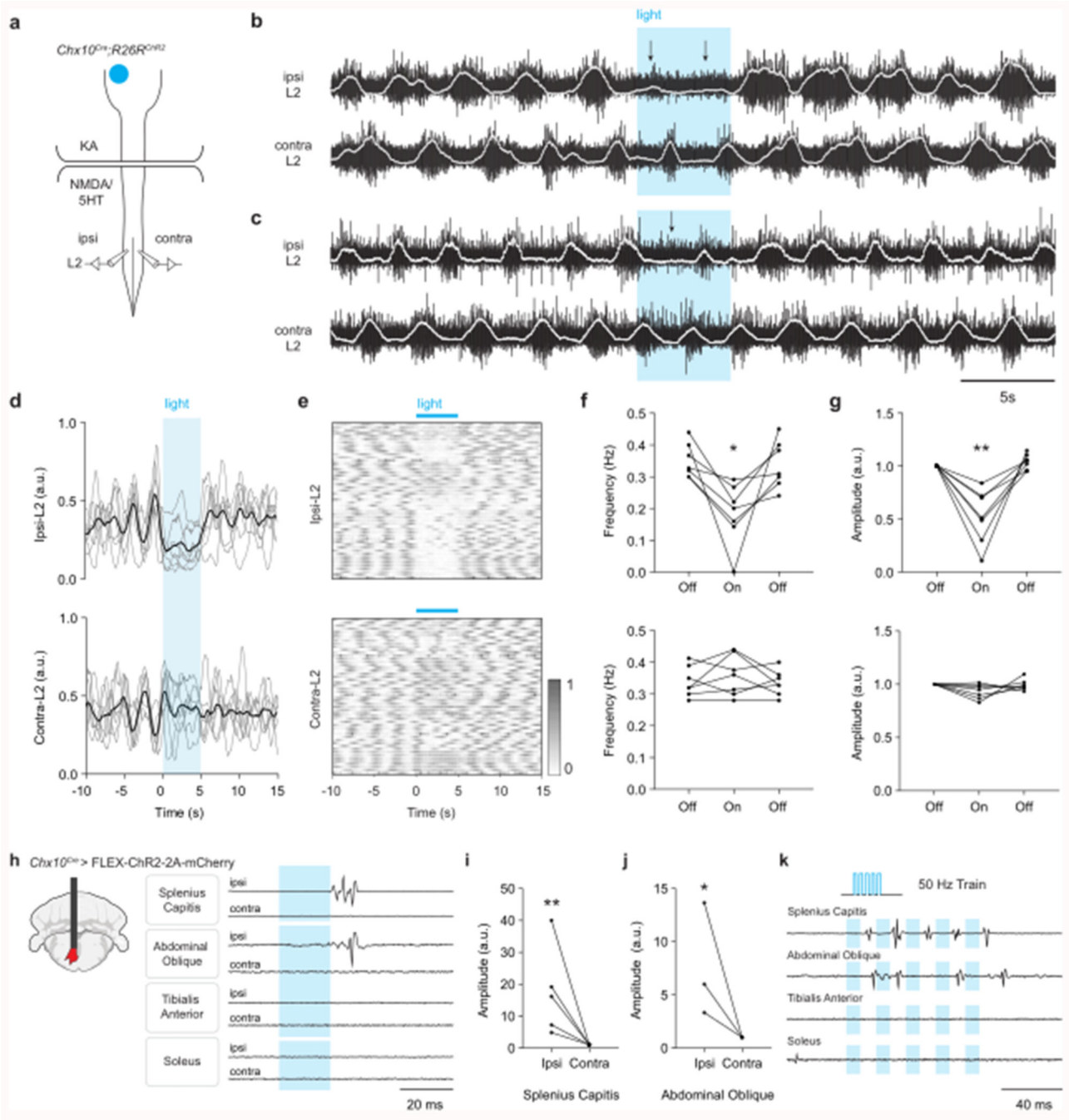

Fig. 4. *Chx10* Gi neurons cause inhibition of ipsilateral rhythmic locomotor activity and excitation of ipsilateral axial muscles.

a, Schematic of split-bath brainstem-spinal cord preparation from P0-4 *Chx10*^{Cre};*R26R*^{ChR2} mice, which was used to interrogate unilateral function of *Chx10* Gi neurons *in vitro*. A rostral brainstem compartment was bathed with kynurenic acid (4 mM) to block all glutamatergic transmission amongst axon collaterals[32], and a caudal spinal cord compartment was bathed with NMDA (6-8 μM) and 5HT (5-15 μM) to induce locomotor-like activity, assayed by recording from the L2 ventral roots. **b-c**, Unilateral

photostimulation of *Chx10* Gi neurons reduced the frequency (**b**) and/or the amplitude (**c**) of locomotor-like activity ipsilateral (ipsi L2) to stimulation with little effect on the contralateral side (contra L2). Traces in (**b**,**c**) are derived from two different mice and are representative of $n = 7$ independent preparations. **d**, Integrated traces normalized in amplitude from 0-1 and averaged across trials for each mouse ($n = 7$ mice, grey), with the grand average across mice represented in black. **e**, 52 trials from 7 mice represented as intensity plots from 0-1, which are integrated traces normalized from 0-1. 3 of the mice represented for ipsi-L2 are also represented in Extended Data Fig. 4. **f**, Quantification of ipsi-L2 and contra-L2 frequency in response to photostimulation. $*P = 0.021$, $n = 7$ mice, one-way repeated measures ANOVA, light-on versus baseline. **g**, Quantification of ipsi-L2 and contra-L2 amplitude in response to photostimulation. $**P = 0.0063$, $n = 7$ mice, one-way repeated measures ANOVA, light-on versus baseline. **h**, Schematic of fiber placement in Gi after injection of AAV-FLEX-ChR2-2A-mCherry in $Chx10^{Cre}$ mice. EMG signals were recorded in axial muscles (splenius capitis or abdominal oblique) and/or hindlimb flexor (tibialis anterior) and extensor (soleus) muscles on the left and right sides of the body. Strong EMG responses could be evoked in the ipsilateral splenius capitis muscle ($n = 5$ mice) and abdominal oblique muscle ($n = 3$ mice). No responses were observed in the hindlimb flexors (tibialis) or extensors (soleus) muscles ($n = 3$ mice). **i**, Quantification of the peak-to-peak response amplitude in the ipsilateral and contralateral splenius capitis muscles. $**P = 0.0022$, ratio paired two-tailed t-test, $n = 5$ mice. **j**, Quantification of the response amplitude in the ipsilateral and contralateral abdominal oblique. $*P = 0.0446$, ratio paired two-tailed t-test, $n = 3$ mice. **k**, Responses in the splenius capitis and abdominal oblique to a high frequency (50 Hz) stimulus train were variable. Motor units did not follow the stimulus train, suggesting a polysynaptic connection between *Chx10* Gi neurons and motor neurons. Traces in (**k**) are representative of $n = 3$ mice for each muscle.

Europe PMC Funders Author Manuscripts

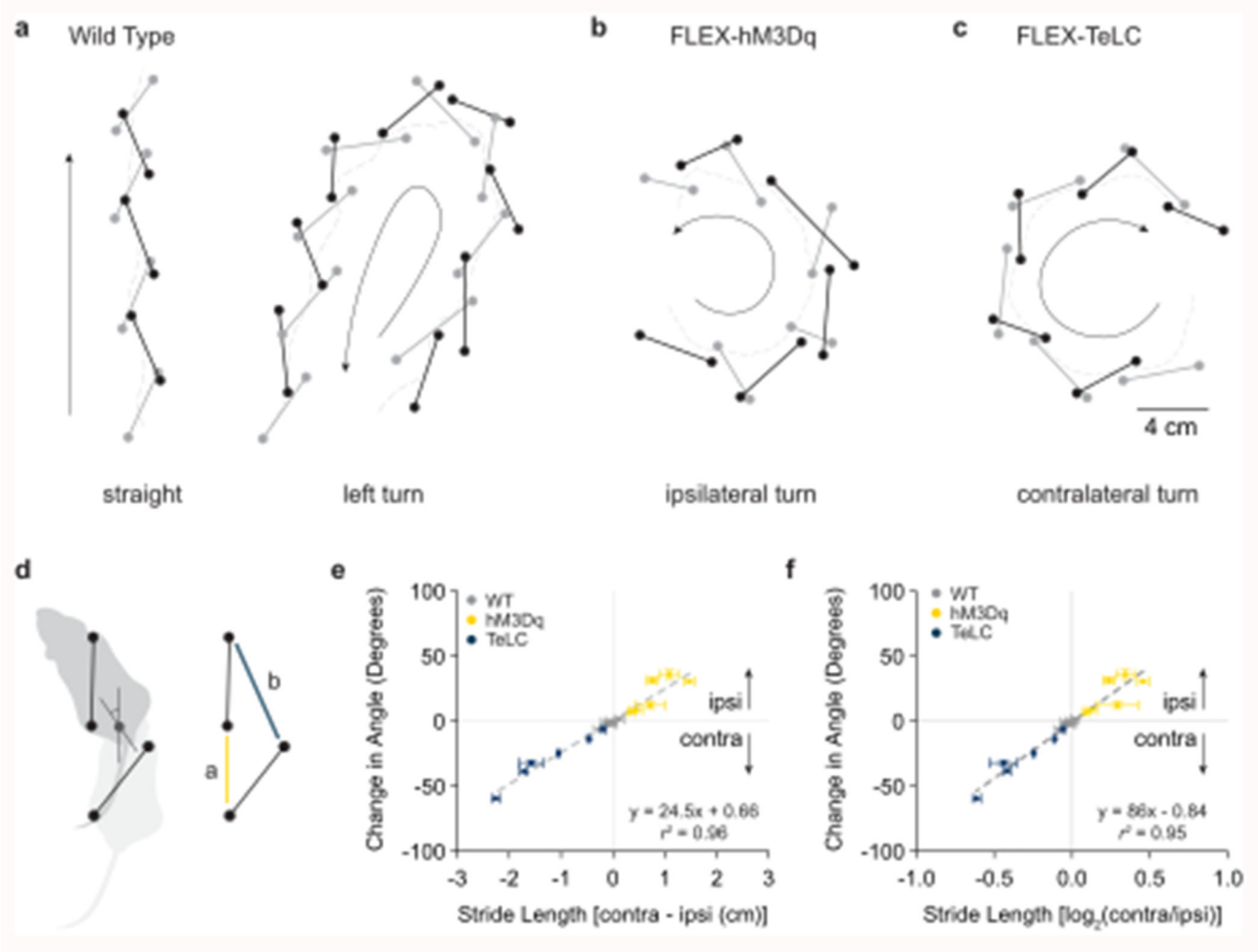

Fig. 5. Limb dynamics during natural and *Chx10*-induced turns.

a, Representative examples of footfalls in a wild-type mouse walking straight and making a spontaneous left turn (n = 6 mice from one experiment). Black lines indicate the left-forelimb/right-hindlimb diagonal, whereas grey lines indicate the right-forelimb/left-hindlimb diagonal. For spontaneous turns, the limb on the side of the turn exhibits shorter steps than its corresponding diagonal. **b**, Representative example of footfalls in a left Gi *Chx10*^{Cre} > FLEX-hM3Dq mouse after injection of CNO (n = 6 mice from two independent experiments), which causes turning toward the ipsilateral (left) side. Steps are shorter on the ipsilateral side. **c**, Representative example of footfalls in a left Gi *Chx10*^{Cre} > FLEX-TeLC mouse (n = 6 mice from two independent experiments), which causes turning toward the contralateral (right) side. Steps are longer on the ipsilateral side. **d**, Schematic of turning based on data in **a-c**. A single step can exhibit left/right motor asymmetry, where the ipsilateral hindlimb exhibits a shorter stride length (a) than the diagonal limb of the contralateral side (b) leading to changes in heading position. **e-f**, Mathematical models demonstrating that a difference in stride length predicts a difference in heading position. We quantified footfalls in wild-type (WT) (n = 6 mice from one experiment), *Chx10*^{Cre} > FLEX-hM3Dq (hM3Dq) (n = 6 mice from two independent experiments), and *Chx10*^{Cre} >

FLEX-TeLC (TeLC) ($n = 6$ mice from two independent experiments). For wild-type mice, the difference in stride length, measured either as the absolute distance (**e**) or as the $\log_2$ ratio (**f**), was close to zero, corresponding to straight walking and/or slight turning to one side. For FLEX-hM3Dq mice after CNO injection, the values are positive—predicting an ipsilateral turn. For FLEX-TeLC mice, the values are negative—predicting a contralateral turn. ***$P < 0.001$ for regression in (**e**) and (**f**), F-test, $n = 18$ mice. Data points in (**e**,**f**) are plotted as mean ± standard error mean. Vertical error bars are omitted in cases where the standard error mean is smaller than the data point itself. Goodness of fit is given as the coefficient of determination (r^2; the square of Pearson's r).

Europe PMC Funders Author Manuscripts

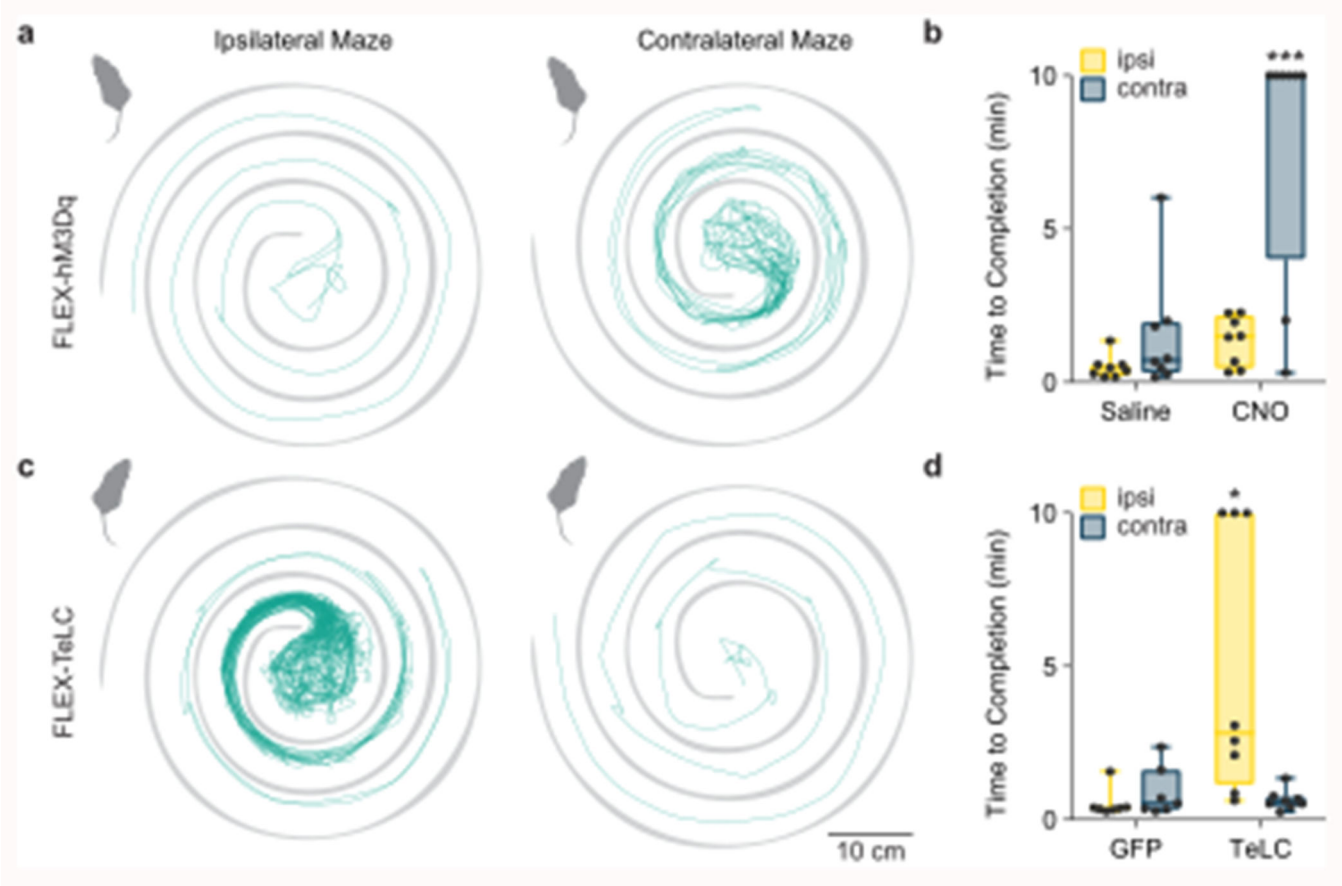

Fig. 6. Unilateral function of *Chx10* Gi neurons is critical for left/right movements during natural exploratory behaviors.

a, Activation of *Chx10* Gi neurons unilaterally with excitatory hM3Dq-DREADDs impairs exploration in a contralateral (right-turn) maze. Turquoise traces represent the movement trajectory of a single representative mouse—the same mouse is represented in both the ipsilateral and contralateral mazes. **b**, 6 of 8 CNO injected mice failed to complete the contralateral maze during a 10 min trial. ***$P < 0.001$, two-way ANOVA with Tukey's multiple comparisons test, $n = 8$ mice from one experiment. **c**, Inhibition of *Chx10* Gi neurons unilaterally with TeLC impairs exploration in an ipsilateral (left-turn) maze. **d**, 3 of 8 TeLC injected mice failed to complete the ipsilateral maze during a 10 min trial. *$P = 0.011$, two-way ANOVA with Tukey's multiple comparisons test, $n = 7$ mice for GFP and $n = 8$ mice for TeLC (one experiment). Box-and-whisker plots in (**b**,**d**) give the median, 25th and 75th percentiles, and range.

Europe PMC Funders Author Manuscripts

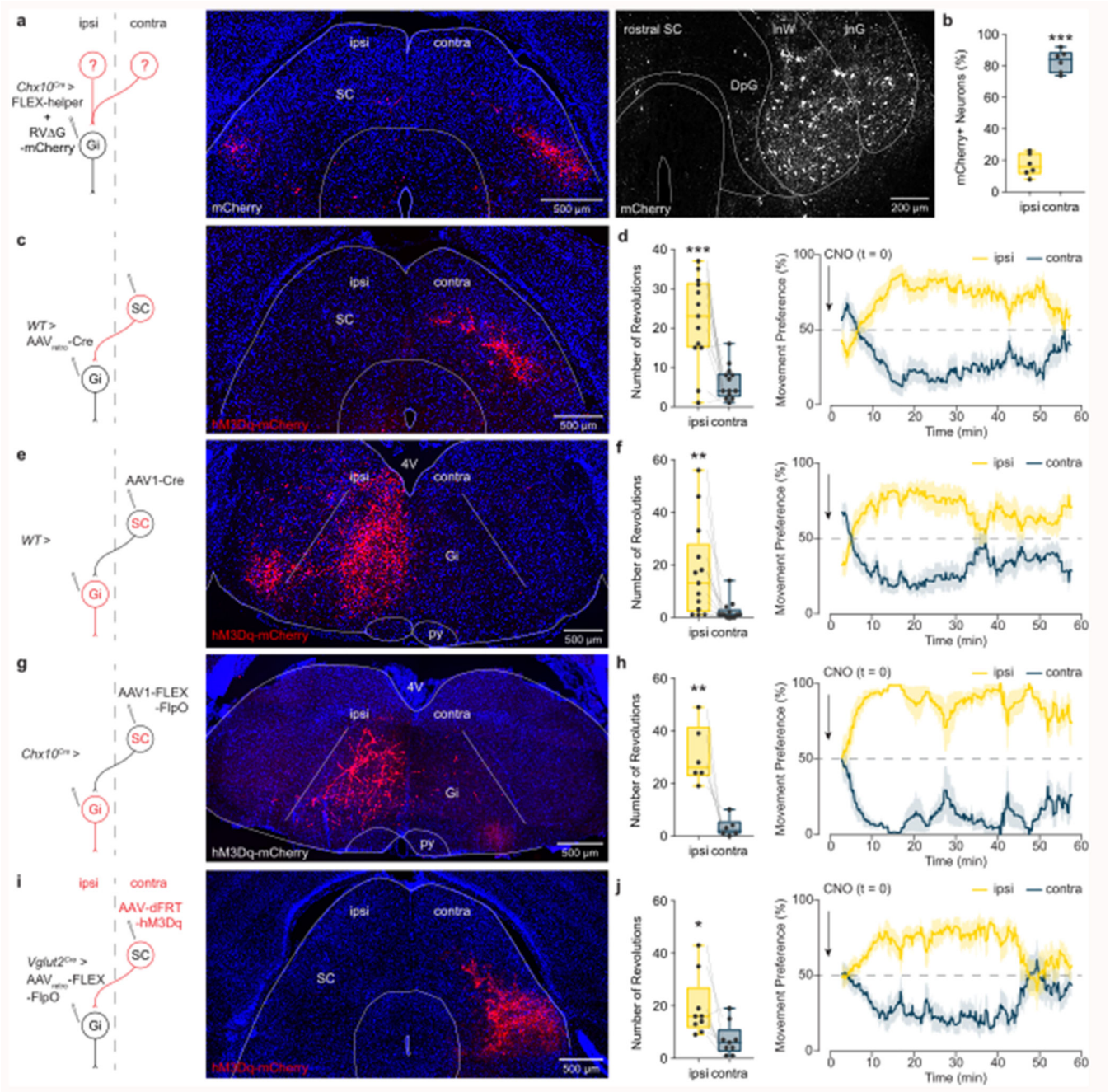

Fig. 7. Contralateral SC steering acts through *Chx10* Gi neurons.

a, A rabies transsynaptic tracing approach was used to identify presynaptic inputs to *Chx10* Gi neurons (see also, Extended Data Fig. 7 and Supplementary Table 2). Rabies-mCherry tracing revealed a prominent input from the contralateral SC, where neurons occupied intermediate layers (*left*, caudal SC; *right*, rostral SC). **b**, Quantification of mCherry-labeled neurons in the ipsilateral and contralateral SC. ***$P < 0.001$, paired two-tailed t-test, $n = 6$ mice from one experiment. **c**, Retrograde behavioral interrogation of the SC-Gi synapse in wild-type mice. Injection of AAV_{retro}-Cre in the Gi caused recombination of a FLEX-hM3Dq-mCherry virus injected in the contralateral SC ($n = 13$ mice). **d**, CNO injection

caused an ipsilateral turning preference. ***$P = 0.0004$, paired two-tailed t-test, $n = 13$ mice from two independent experiments. *Right*, Instantaneous quantification of turning percentage after CNO injection. **e**, Anterograde behavioral interrogation of the SC-Gi synapse in wild-type mice. Injection of AAV1-Cre in the contralateral SC caused recombination of a FLEX-hM3Dq-mCherry virus injected in the ipsilateral Gi ($n = 13$ mice). **f**, CNO injection caused an ipsilateral turning preference. **$P = 0.0087$, paired two-tailed t-test, $n = 13$ mice from two independent experiments. *Right*, Instantaneous quantification of turning percentage after CNO injection. **g**, Anterograde behavioral interrogation of the SC-Gi synapse in $Chx10^{Cre}$ mice. Injection of AAV1-FLEX-FlpO in the contralateral SC caused recombination of a dFRT-hM3Dq-mCherry virus injected in the ipsilateral Gi ($n = 6$ mice). **h**, CNO injection caused an ipsilateral turning preference. **$P = 0.0053$, paired two-tailed t-test, $n = 6$ mice from two independent experiments. *Right*, Instantaneous quantification of turning percentage after CNO injection. **i**, Retrograde behavioral interrogation of the SC-Gi synapse in $Vglut2^{Cre}$ mice. Injection of AAV_{retro}-FLEX-FlpO in the Gi caused recombination of a dFRT-hM3Dq-mCherry virus injected in the contralateral SC ($n = 9$ mice). **j**, CNO injection caused an ipsilateral turning preference. *$P = 0.0113$, paired two-tailed t-test, $n = 9$ mice from two independent experiments. *Right*, Instantaneous quantification of turning percentage after CNO injection. Box-and-whisker plots in (**b**,**d**,**f**,**h**,**j**) give the median, 25^{th} and 75^{th} percentiles, and range. Time-series data in (**d**,**f**,**h**,**j**) are plotted as mean ± standard error mean.